



GEOLOGY FOR SOCIETY

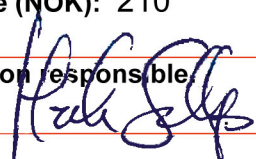
SINCE 1858



**GEOLOGICAL
SURVEY OF
NORWAY**

· NGU ·



Report no.: 2015.030		ISSN: 0800-3416 (print) ISSN: 2387-3515 (online)		Grading: open report	
Title: Mineralization styles and formation temperatures of the Knaben molybdenum deposits, southern Norway					
Authors: Axel Müller, Iain Henderson, Charles Jourdan, Trond Slagstad			Client: NGU		
County: Rogaland			Commune: Kvindalen		
Map-sheet name (M=1:250.000) Mandal			Map-sheet no. and -name (M=1:50.000) Fjotland 1412-3		
Deposit name and grid-reference: Knaben mining district			Number of pages: 59		Price (NOK): 210
Fieldwork carried out: 19.09-26.09.2013			Date of report: 31.09.2015		Map enclosures: -
Fieldwork carried out: 19.09-26.09.2013			Date of report: 31.09.2015		Project no.: 352800
Fieldwork carried out: 19.09-26.09.2013			Date of report: 31.09.2015		Person responsible: 
Summary: <p>The report documents the lithologies and molybdenite mineralization exposed in underground mines of the Knaben molybdenum (Mo) mining district in Kvinesdal, Rogaland, SW Norway. Scanning electron microscope cathodoluminescence (SEM-CL) and trace element analyses of quartz by laser ablation inductively coupled mass spectrometry (LA-ICP-MS) were performed on 37 quartz and quartz-bearing samples in order to better understand the P-T conditions during magma emplacement and Mo mineralization. The major rock type in the Knaben district is weakly foliated, porphyritic reddish biotite granite with an intrusion age of c. 1036 Ma belonging to the Mesoproterozoic Sirdal Magmatic Belt. The porphyritic granite contains mega screens and xenoliths of amphibolite and flaser gneiss in an area >10 km long (N-S) and 1 km wide (E-W). In the Knaben 2 and Ørnehommen mines the porphyritic granite is intruded by grey, quartz-rich granite with disseminated molybdenite. Latter is assumed to be the primary source of molybdenum. Coarse-grained molybdenite mineralization is commonly associated with ductile deformed, pegmatitic quartz bands and in one case with a large (300x150x5 m) pegmatite (Kvina mine). The quartz of almost all investigated mineralized and non-mineralized rock types shows CL features which are typical for igneous quartz. The bright luminescent igneous quartz is superimposed by several generations of secondary quartz with low CL intensity. The generally low abundance of secondary structures suggests that the amount of circulating, late- to post-magmatic fluids was relative limited. The most distinctive secondary CL structures are oscillatory growth fronts bulging into and replacing bright luminescent primary quartz by grain boundary migration. The structures are interpreted as solid-solution replacement textures and developed post-magmatically during high temperatures. The temperatures remained high over a relative long period allowing the development of these rare textures. Because these textures are omnipresent in all investigated igneous rocks in the Knaben district, they indicate a regional high-temperature event likely caused by long-lasting heat flow and fluid circulation as a result of voluminous, long-lived (c. 1060 to 920 Ma) magmatism related to the Sirdal Magmatic Belt and Hornblende-Biotite Granite Suite. Al, Ti, Li, and Ge concentrations in quartz of igneous rocks of the Knaben mining district show a wide scatter. Correlations between these elements are only rudimentarily developed and presumably disturbed by late- to post-magmatic processes as described above. The application of the Ti-in-quartz-geothermobarometer indicates that the rocks associated with the molybdenite mineralization were formed at magmatic conditions at c. 4 kbar. The crystallization temperature of the grey, quartz-rich granite with disseminated molybdenite was 733±21°C and that of the pegmatitic quartz bands with coarse-grained molybdenite mineralization was 714±46°C. However, the Ti content of the mineralized quartz bands decreases from south towards north corresponds to a temperature change from 782±13°C (Bragold mine) to 673±29°C (Knaben 1 and Synnøve mines). This change may be reflect a continuous temperature gradient of the molybdenite mineralization across the Knaben mining district.</p>					
Keywords:		Scientific report		Knaben	
Quartz		Molybdenite		Sirdal Magmatic Belt	

Content

1. Introduction	7
2. Samples and methods	11
2.1 Sample preparation	11
2.2 Scanning electron microscope cathodoluminescence imaging	11
2.3 Laser ablation inductively coupled plasma mass spectrometry	11
3. Major lithologies of the Knaben mining district – an introduction	12
4. Description of macroscopic mineralization styles	14
4.1 Kvina mine	14
4.2 Knaben 1 mine	17
4.3 Synnøve 3 mine	19
4.4 Spillebrok-skjærpene, east tunnel	20
4.5 Roma mine, upper north tunnel	21
4.6 Roma mine, upper south tunnel	23
4.7 Roma mine, lower tunnel “Grundstollen”	25
4.8 Ørnehommen mine	27
4.9 Jelå mine, upper tunnel	29
4.10 Knaben 2 mine	30
4.11 Bragold mine	35
4.12 Hommen mine	35
5. Summary of observed types of mineralization	37
6. Results	40
6.1 Cathodoluminescence-contrasted structures in quartz	40
6.2 Quartz chemistry	45
6.2 Application of the titanium-in-quartz geothermobarometry	49
7. Summary and outlook	50
8. References	52

Figures

Figure 1a. Map of Sveconorwegian domains (sectors and terranes), major magmatic units and Mo mineralization of south Norway. The inset shows the location of the Knaben zone (KZ) within in the Sirdal Magmatic Belt (from Slagstad et al. unpublished). HBG – hornblende-biotite granite suite 0.98-0.93 Ga.	8
Figure 1b. Simplified structural-geological map of the Knaben Zone, showing the most important structures, lithologies, and the xenolith screens. ECC - Extensional crenulation cleavage. From Stormoen (2015).	10
Figure 2. A - Topographic map Vest Agder in southwest Norway with the location of the map shown in B. B – The Knaben mining district with locations of molybdenite mines investigated in this study. Modified from Stormoen (2015).	10
Figure 3. Hand specimen showing the contact between porphyritic reddish biotite granite (left) and flaser gneiss (right) from the Roma mine, upper north tunnel (sample 26091304). The scale corresponds to 1 cm.	12
Figure 4. Hand specimen showing the contact between porphyritic reddish biotite granite (right) and mineralized, grey quartz-rich granite (left) from the Ørnehommen mine, upper tunnel (sample 25091306). The scale corresponds to 1 cm.	13
Figure 5. Simplified scheme of lithologies and mineralization styles exposed in the Kvina mine. The red disks indicate the location of coarse-grained molybdenite mineralization. The numbers correspond to sample numbers (see also Appendix 1).	15
Figure 6. Hand specimen of deformed and mineralized pegmatite from the Kvina mine (sample 21091306a). bt – biotite, kfs – K-feldspar, mo – molybdenite, qtz - quartz.	16

Figure 7. Hand specimen of deformed and mineralized pegmatite from the Kvina mine (sample 21091306b). kfs – K-feldspar, mo – molybdenite, qtz - quartz.	17
Figure 8. Simplified scheme of lithologies and mineralization styles exposed in the Knaben I mine. The late, cross-cutting pegmatite stopped during emplacement at the contact between flaser gneiss and amphibolite due to the lithological contrasts and not because it was “cut” by the amphibolite. The red disks indicate the location of coarse-grained molybdenite mineralization. The numbers correspond to sample numbers (see also Appendix 1).	18
Figure 9. Hand specimen of an aplitic feldspar vein with coarse-grained molybdenite (sample 24091310).	19
Figure 10. Simplified scheme of lithologies and mineralization styles exposed in the Synnøve 3 mine. The red disks indicate the location of coarse-grained molybdenite mineralization and the red dots that of fine-grained, disseminated molybdenite mineralization. The numbers correspond to sample numbers (see also Appendix 1).	20
Figure 11. Simplified scheme of lithologies and mineralization styles exposed in the eastern tunnel of the Spillebrok-skjærpenne. The red disks indicate the location of coarse-grained molybdenite mineralization related to pegmatitic quartz bands. The numbers correspond to sample numbers (see also Appendix 1).	21
Figure 12. Simplified scheme of lithologies and mineralization styles exposed in the Roma mine, upper north tunnel. The red disks indicate the location of coarse-grained molybdenite mineralization related to pegmatitic quartz bands. The numbers correspond to sample numbers (see also Appendix 1).	22
Figure 13. Hand specimen showing diffuse contact between reddish porphyritic granite (upper right) and biotite-rich granite of presumably granodioritic composition (sample 26091306). The scale corresponds to 1 cm.	23
Figure 14. Simplified scheme of lithologies and mineralization styles exposed in the Roma mine, upper south tunnel. The red disks indicate the location of coarse-grained molybdenite mineralization related to pegmatitic quartz bands. The numbers correspond to sample numbers (see also Appendix 1).	24
Figure 15. Hand specimen showing a pegmatitic quartz band (pg1) with coarse-grained molybdenite mineralizations (mo) at the upper and lower contact (sample 20091306b). The quartz band occurs in migmatized amphibolite (amph). A late, undeformed, non-mineralized, K-feldspar-rich pegmatite vein (pg2) crosscut with low angle the foliation of the amphibolite and quartz band. The scale corresponds to 1 cm.	25
Figure 16. Simplified scheme of lithologies and mineralization styles exposed in the Roma mine, lower tunnel. The red disks indicate the location of coarse-grained molybdenite mineralization related to pegmatitic quartz bands and the red dots that of fine-grained, disseminated molybdenite mineralization. The numbers correspond to sample numbers (see also Appendix 1).	26
Figure 17. Simplified scheme of lithologies and mineralization styles exposed in the Ørnehommen mine. The red disks indicate the location of coarse-grained molybdenite mineralization related to pegmatitic quartz bands and the red dots that of fine-grained, disseminated molybdenite mineralization. The numbers correspond to sample numbers (see also Appendix 1).	28
Figure 18. Hand specimen showing the diffuse contact between non-mineralized, fine-grained and medium-grained, weakly porphyritic biotite granite. Ørnehommen lower tunnel, sample 25091301. The scale corresponds to 1 cm.	29
Figure 19. Simplified scheme of lithologies and mineralization styles exposed in the Jelå mine, upper tunnel. The red disks indicate the location of coarse-grained molybdenite mineralization related to pegmatitic quartz bands. The numbers correspond to sample numbers (see also Appendix 1).	30

Figure 20. Simplified scheme of lithologies and mineralization styles exposed in the Knaben 2 mine. The red disks indicate the location of coarse-grained molybdenite mineralization related to pegmatitic quartz bands and the red dots that of fine-grained, disseminated molybdenite mineralization. The numbers correspond to sample numbers (see also Appendix 1).	32
Figure 21. Hand specimen of grey, quartz-rich mineralized granite with changing grain size. The sample shows a foliation-concordant pegmatitic quartz band (center of image) with a biotite layer at the lower contact (sample 19091301a). The scale corresponds to 1 cm. ...	33
Figure 22. Hand specimen of grey, aplitic, mineralized granite interlayered with pegmatitic quartz bands with coarse-grained molybdenite mineralization (sample 19091301b). The scale corresponds to 1 cm.	33
Figure 23. Hand specimen of grey granite with coarse-grained molybdenite fracture filling. Knaben 2 mine, sample 24091101. The edges of the squares on the scale corresponds to 2 cm.	34
Figure 24. Simplified scheme of lithologies and mineralization styles exposed in the Bragold mine. The red disks indicate the location of coarse-grained molybdenite mineralization related to pegmatitic quartz bands. The numbers correspond to sample numbers (see also Appendix 1).	35
Figure 25. Simplified scheme of lithologies and mineralization styles exposed in the Hommen mine. The red disks indicate the location of coarse-grained molybdenite mineralization related to pegmatitic quartz bands and the red dots fine-grained disseminated molybdenite mineralization in moderately deformed porphyritic granite. The number corresponds to sample numbers (see also Appendix 1).	36
Figure 26. Hand specimen of pegmatitic quartz with minor molybdenite and massive chalcopyrite. Hunsbedt Skjærp, sample 20091317. The scale corresponds to 1 cm.	38
Figure 27. BSE images of the chalcopyrite-chamosite-apatite mineralization overprinting pegmatitic quartz bands with molybdenite mineralization. Hunsbedt Skjærp, sample 20091315. A – Overview image. B – Detailed image. Mineral abbreviations: ap – apatite, chm – chamosite, ccp - chalcopyrite.	39
Figure 28. SEM-CL images of quartz. A – Igneous quartz of non-mineralized porphyritic granite from the Synnøvre 3 mine, sample 20091308, with bright CL and a network of fractures healed with non-luminescent quartz (sqtz1). B – Close up of a healed fracture (black) containing fluid inclusions. Mineralized pegmatitic quartz band from the Knaben 1 mine. Sample 20091314. C – BSE image of the same crystal as shown in (B) visualizing the holes of decrepitated fluid inclusions which are located within the non-luminescent domains shown in (B). D – Quartz with bright CL with several types of secondary structures (sqtz1 to sqtz3). See text for explanation. Mineralized grey granite from the Knaben 2 mine. Sample 26091311. E – Quartz with bright CL with several types of secondary structures (sqtz1 to sqtz3). See text for explanation. Pegmatite quartz of the Kvina mine. Sample 21091309. D – Quartz with bright CL and a few secondary structures (sqtz1 to sqtz3). See text for explanation. Flaser gneiss of the Knaben 1 mine. Sample 20091313.	41
Figure 29. SEM-CL image of a hydrothermal quartz crystals of late, brittle faults exposed in the lower Roma mine (sample 25091307). The crystal shows a distinct primary oscillatory growth zoning (straight banding) overprinted by irregular network of healed, non-luminescent (black) micro fractures connecting micro domains of non-luminescent quartz around fluid inclusions.	42
Figure 30. SEM-CL images of secondary quartz sqtz4 replacing adjacent crystals of primary quartz (pqtz) by grain boundary migration. The growth (replacing) direction is indicated by white arrows. A, B, C, D and F - Non-mineralized, undeformed pegmatite from the	

<i>Knaben 2 mine. Sample 26091308. E –Mineralized pegmatitic quartz band from the Bragold mine. Sample 23091311.</i>	43
Figure 31. SEM-CL (A, C, D) and BSE (B, D, F) images of quartz of the Hunsbedt Skjærp. The images illustrate how the chalcopyrite (ccp)- chamosite (chm) – apatite (ap) assemblage replaces primary quartz (pqtz) related to the molybdenite mineralization. Minor dull luminescent quartz (sqtz5a and sqtz5b) related to the chalcopyrite mineralization overgrew the primary quartz, by forming sub-euhedral crystals (sqtz5a) with growth zoning (white arrows) or dendritic crystals intergrowth with chamosite (sqtz5b). The black arrow in (E) indicates the boundary between primary and secondary quartz overgrowth.	44
Figure 32. Graph showing Al versus Ti concentrations of investigated quartz samples. Concentrations were determined with LA-ICP-MS.	46
Figure 33. Graph showing Al versus Li concentrations of investigated quartz samples. Concentrations were determined with LA-ICP-MS. The red dashed line corresponds the Al-Li correlation line $Li (ppm) = 0.2133 \times Al (ppm)$ of quartz of the Borborema pegmatites, Brazil, which represents a Li-rich magmatic system (Beurlen et al. 2011).	46
Figure 34. Graph showing the Al concentration versus Ge/Ti ratio of investigated quartz samples. According to Jacamon and Larsen (2009) the Ge/Ti ratio of quartz is an index of the magmatic evolution of granitic igneous systems and, thus, should increase with increasing Al. However, in the case of the Knaben samples no clear trend is developed. Concentrations were determined with LA-ICP-MS.	47
Figure 35. Graph showing the variation of the Ti content of mineralized quartz bands (primary quartz = pqtz) in relation to their N-S location. There seems to be a systematic decrease of the Ti content from the south (Bragold mine) towards north (Knaben 1 and Synnøve mines). Quartz of the chalcopyrite-molybdenite mineralization at Hunsbedt Skjærp (red ellipse) and Kvina mine (green ellipse) do not follow this trend.	47

Tables

Table 1. Simplified classification of macroscopic observed structural styles of molybdenite mineralization in underground mines of the Knaben mining district.	37
Table 2. Average concentrations of trace elements (in ppm) in quartz determined with LA-ICP-MS. Numbers in parentheses correspond to the number of analyses. STD – standard deviation.	48
Table 3. Crystallization temperatures of quartz of different rock types of the Knaben mining district. The temperatures were calculated using the Ti-in-quartz geothermobarometer by Huang and Audétat (2012). The applied pressure was 4.0 ± 0.2 kbar based on Al-in-hornblende barometry (Coint et al. 2015). STD – standard deviation.	49

Appendix

Appendix 1. Sample list. Mineral abbreviations: ccp – chalcopyrite, kfs – K-feldspar, mo – molybdenite, py- pyrite, qtz – quartz.	52
Appendix 2. Trace element concentrations (in ppm) of quartz determined with LA-ICP-MS. Two analyses (A and B) were performed on each sample. Concentrations of Na, K, and Ca above the limit of detection (LOD) are caused by fluid inclusions. Rock type abbreviations: fgn – flaser gneiss, ggr – mineralized grey granite, hqtz – hydrothermal quartz of late fractures, mo-qtz – mineralized pegmatitic quartz bands, ngr - non-mineralized granites except prophyritic granite, pegd - non-mineralized pegmatite dykes, peg – Kvina pegmatite, pgr – porphyritic granite.	58

1. Introduction

The report documents field observations of the style of molybdenite mineralization and related lithologies exposed in underground mines of the Knaben mining district in Kvinesdal, Rogaland, SW Norway (Figures 1a, 1b, 2). The Knaben district belongs to the Sveconorwegian Rogaland-Vest Agder molybdenum (Mo) province which is characterized by common small syn- to late orogenic (post-peak metamorphism) vein-type, disseminated and stratiform or stratabound Mo deposits, mined at the beginning of the 20th century (Bugge 1963; Sandstad 2012). The Knaben district is the most important among them and, mined at small scale until today, is one of the historically important Mo mining districts in Europe. A total of c. 8.5 Mt of ore was extracted with an average grade of c. 0.2 % (Bugge 1963).

Locations of the underground mines investigated in this study are shown in Figure 2. A detailed description of the mines is given by Jourdan (2003). The field work was carried out between 19th and 26th September 2013. 77 rock samples were collected (Appendix 1). Macroscopic mineralization styles of the investigated mines are described together with the type and origin of the samples. Scanning electron microscope cathodoluminescence (SEM-CL) and trace element analyses of quartz by laser ablation inductively coupled mass spectrometry (LA-ICP-MS) were performed on 37 quartz-bearing rock samples in order to better understand the P-T conditions during magma emplacement and molybdenite mineralization by applying the Ti-in-quartz geothermobarometer (Huang and Audétat 2012).

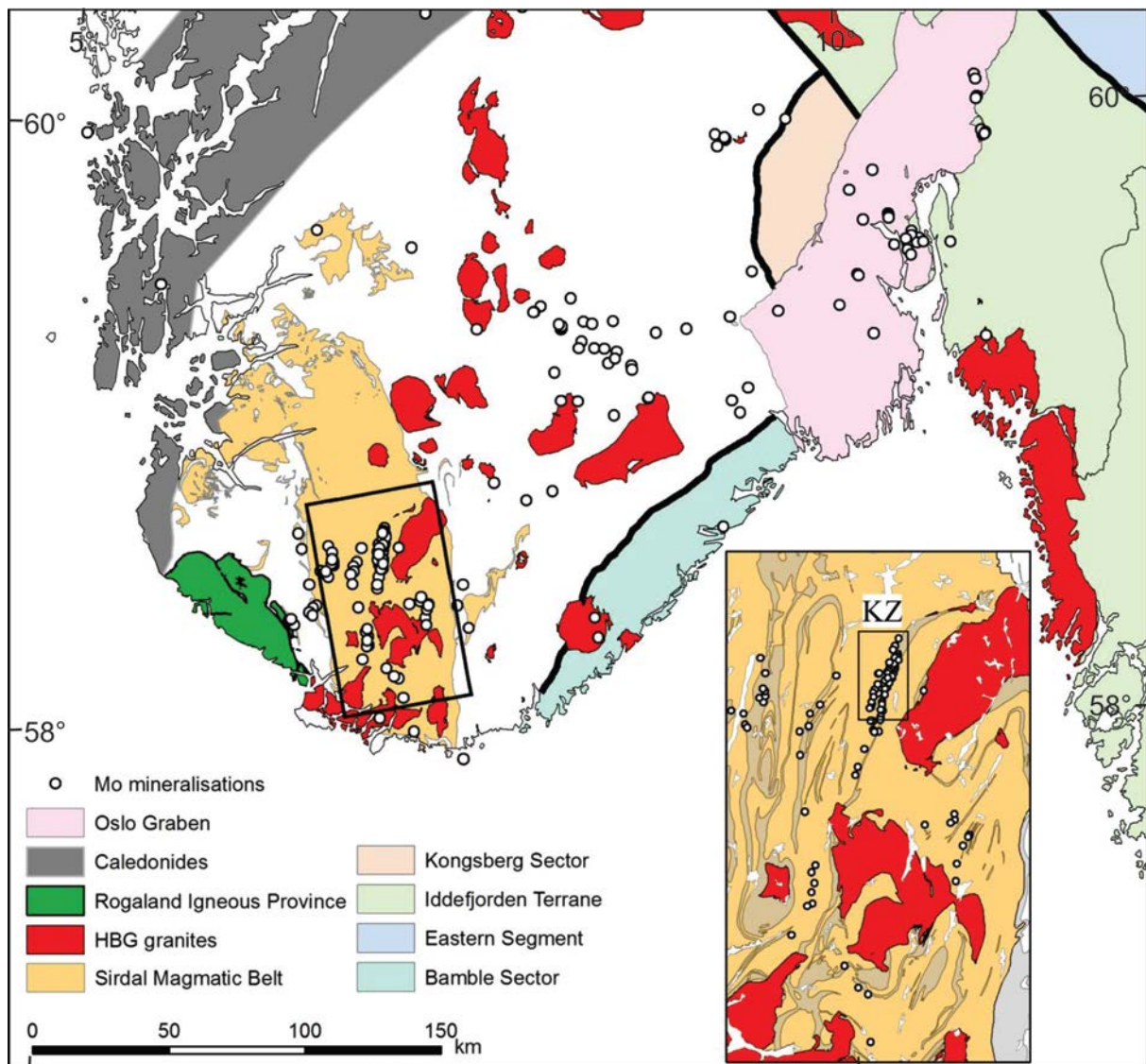


Figure 1a. Map of Sveconorwegian domains (sectors and terranes), major magmatic units and Mo mineralization of south Norway. The inset shows the location of the Knaben zone (KZ) within in the Sirdal Magmatic Belt (with permission from Trond Slagstad; unpublished). HBG – hornblende-biotite granite suite 0.98-0.93 Ga.

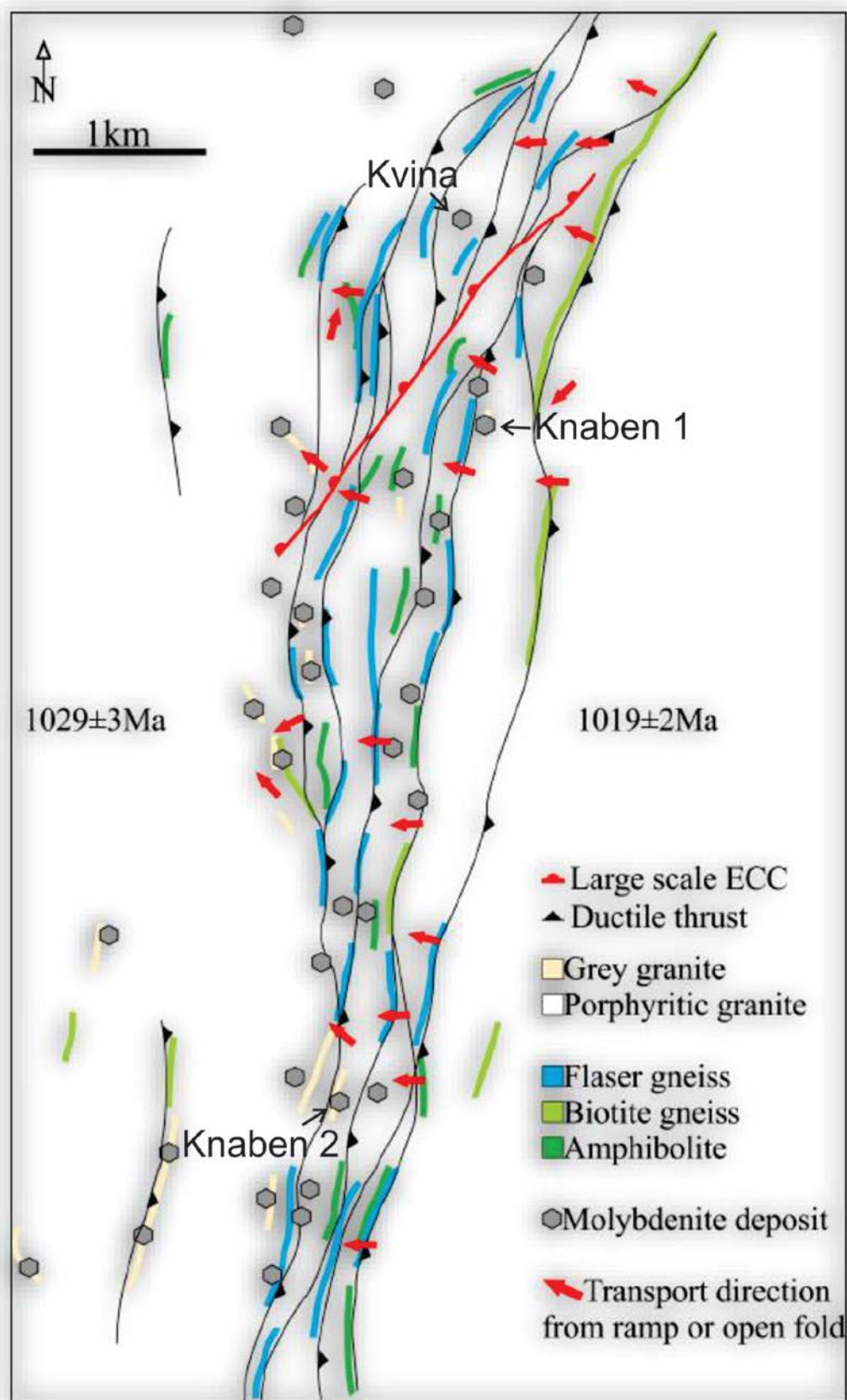


Figure 1b. Simplified structural-geological map of the Knaben Zone, showing the most important structures, lithologies, and the xenolith screens. ECC - Extensional crenulation cleavage. From Stormoen (2015).



Figure 2. A - Topographic map Vest Agder in southwest Norway with the location of the map shown in B. B – The Knaben mining district with locations of molybdenite mines investigated in this study. Modified from Stormoen (2015).

2. Samples and methods

2.1 Sample preparation

37 quartz-bearing samples out of 77 collected rock samples were chosen for cathodoluminescence and trace element analyses of quartz (Appendix 1). Petrological surface-polished, thick (300 μm) sections were prepared at the Geological Survey of Norway in Trondheim. The sections were mounted with Epoxy on a $4.8 \times 2.8 \times 0.2$ cm large glass slide.

2.2 Scanning electron microscope cathodoluminescence imaging

Scanning electron microscope cathodoluminescence (SEM-CL) images of quartz were obtained with Centaurus BS Bialkali CL detector attached to the LEO 1450VP analytical SEM. The investigations were carried out on carbon-coated thick sections, the same sections which were used for LA-ICP-MS. The applied acceleration voltage and current at the sample surface were 20 kV and ~ 2 nA, respectively. SEM-CL images were collected from one scan of 43 s photo speed and a processing resolution of 1,024 x 768 pixels and 256 grey levels.

SEM-CL imaging reveals micro-scale (<1 mm) growth zoning, alteration structures and different quartz generations which are not visible with other microscopic methods. Grey-scale contrasts are caused by the heterogeneous distribution of lattice defects (e.g., oxygen and silicon vacancies, broken bonds) and lattice-bound trace elements (e.g., Götze et al. 2001). Although the physical background of the quartz CL is not fully understood, the structures revealed by CL give information about crystallization, deformation and alteration.

2.3 Laser ablation inductively coupled plasma mass spectrometry

Concentrations of Li, Be, B, Al, P, Ti, Ca, Na, K, Mn, Fe, and Ge were analyzed in situ by LA-ICP-MS. The analyses were performed on the double-focusing sector field mass spectrometer model ELEMENT XR ICP-MS with an attached New Wave UP193FX Excimer 193-nm laser probe. The laser had a repetition rate of 15 Hz, a speed of $15 \mu\text{m s}^{-1}$, a spot size of $75 \mu\text{m}$, and energy fluence of about 14 mJ cm^{-2} on the sample surface. Raster ablation was applied in the centre of quartz crystals on an area of approximately $250 \times 500 \mu\text{m}$. The approximate depth of ablation was between 40 and $100 \mu\text{m}$ depending on the crystallographic orientation and absorption behavior of the individual quartz crystals. A Hitachi CCD video camera type KP-D20BU attached to the laser system facilitates the observation of the laser ablation process to avoid the analysis of micro mineral and fluid inclusions ($>0.1 \mu\text{m}$) occurring commonly in natural quartz. The carrier gas for transport of the ablated material to the ICP-MS was He mixed with Ar. External calibration was performed using four silicate glass reference materials (NIST SRM 610, 612, 614, 616), the NIST SRM 1830 soda-lime float glass, the BAM No.1 amorphous SiO_2 glass and the synthetic pure quartz monocrystal Qz-Tu. Certified, recommended and proposed values for these reference materials were taken from the certificates of analysis where available, or otherwise from Jochum et al. (2011). The isotope ^{29}Si was used as the internal standard. A linear regression model, including several measurements of the different reference materials, was used to define the calibration curve for each element. For the calculation of P concentrations, the procedure of Müller et al. (2008) was applied. Ten sequential measurements on the “ SiO_2 blank” crystal were used to estimate the limits of detection (LOD) which were based on $3\times$ standard deviation (3σ) of the ten measurements. LODs vary for each analysis sequence (measurement day). Examples of LODs are given in Appendix 2. The analytical error ranges within 10% of the absolute concentration of the element. Detection limits for the alkali metals Na, K, and Ca are relatively high compared to other elements because they are difficult to measure with the LA-ICP-MS system. More details of the measurement procedure are provided by Flem et al. (2002) and Flem and Müller (2012).

3. Major lithologies of the Knaben mining district – an introduction

The major host rock of the Knaben molybdenite mineralization is weakly foliated, porphyritic medium- to coarse-grained, reddish biotite granite (referred to as red granitic gneiss by Bingen et al. 2015) with an intrusion age of c. 1036 Ma belonging to the Mesoproterozoic Sirdal I-type Magmatic Belt (e.g., Slagstad et al. 2013; Bingen et al. 2015; Coint et al., 2015). The granite is metaluminous to peraluminous and has relative high-K content ($68 < \text{SiO}_2 < 77$ wt.%; Lysberg 1976; Stormoen 2015).

Within the Knaben mining district the reddish porphyritic granite contains commonly meter-scale ductile deformed xenoliths and screens of amphibolite and granitic flaser gneiss (Figure 3). The latter is also referred to as augen gneiss by Bingen et al. (2015) with a protolith age of 1257 ± 6 Ma. (The name augen gneiss is misleading because the structure of the reddish porphyritic granite resembles more a classical augen gneiss texture than the flaser gneiss [compare Figures 3 and 4].) This pre-Sveconorwegian orthogneiss was formed during a regional-scale bimodal magmatic event at 1285-1250 Ma in the Telemark Terrane (Bingen et al. 2015). The size of enclaves ranges from several meters to several hundred of meters and cluster in a >10 km long (N-S) and 1 km wide belt in which the majority of Mo mineralization occurs. The enclaves are aligned concordant to the generally N-S striking, c. 30° E-dipping foliation. This local mixture of lithologies in the >10 km long belt is referred to as “Knaben gneiss” by Lysberg (1976). (The term “Knaben gneiss” should not be used because it represents a mixture of different rock types, with intrusive contacts. The “Knaben gneiss” is, in fact, a zone rich in screens and xenoliths of metamorphic rocks, intruded by porphyritic granite (Coint et al. 2015), and most likely represents a contact zone between two sheet-like granitic plutons [Stormoen 2015]).

In the Knaben 2 and Ørnehommen mines the porphyritic granite is intruded by a up to 15 m thick sheet of grey, medium-grained, quartz-rich granite (referred to as grey leucogneiss by Bingen et al. 2015) commonly containing fine-grained, disseminated molybdenite. Silica content of the grey granite varies between 73.5 and 81.0 wt.% and K_2O between 5.0 and 5.9 wt.% (9 analyses; Lysberg 1976). The intrusion age is 1036 ± 6 Ma (Bingen et al. 2015) and is therewith coeval with the reddish porphyritic granite both being different facies of the same large pluton. Coarse-grained molybdenite is commonly associated with ductile deformed, pegmatitic quartz bands (0.5 to 20 cm wide and up to several meters long) hosted by the reddish granite and in one case with a large scale pegmatite (Kvina mine). The quartz bands contain minor recrystallized feldspar and biotite.

The entire sequence is cross-cut by undeformed (“late”) and non-mineralized pegmatite dykes. In most of the mines these steeply dipping pegmatite dykes are foliation-discordant. Only in the Knaben 2 mine foliation-concordant undeformed pegmatites of this type occur.

The formation of the Knaben Mo deposits has been most recently considered to be magmatogenic (Stormoen 2015 and this study). According to the magmatogenic model, Mo is transported via the granite magmas and hydrothermal fluids released from these magmas at and after the main magmatic event at c. 1036 Ma. Deposits formed after 1036 Ma imply younger mineralizing magmatic batches or a reworking of previously formed mineralization (Bingen et al. 2015). In addition, an alternative metamorphogenic model has been proposed by Bingen et al. (2015), in which Mo is derived from the screens and xenoliths, transported via hydrothermal fluids and concentrated locally where sulphur was available.



Figure 3. Hand specimen showing the contact between porphyritic reddish biotite granite (left) and flaser gneiss (right) from the Roma mine, upper north tunnel (sample 26091304). The scale corresponds to 1 cm.

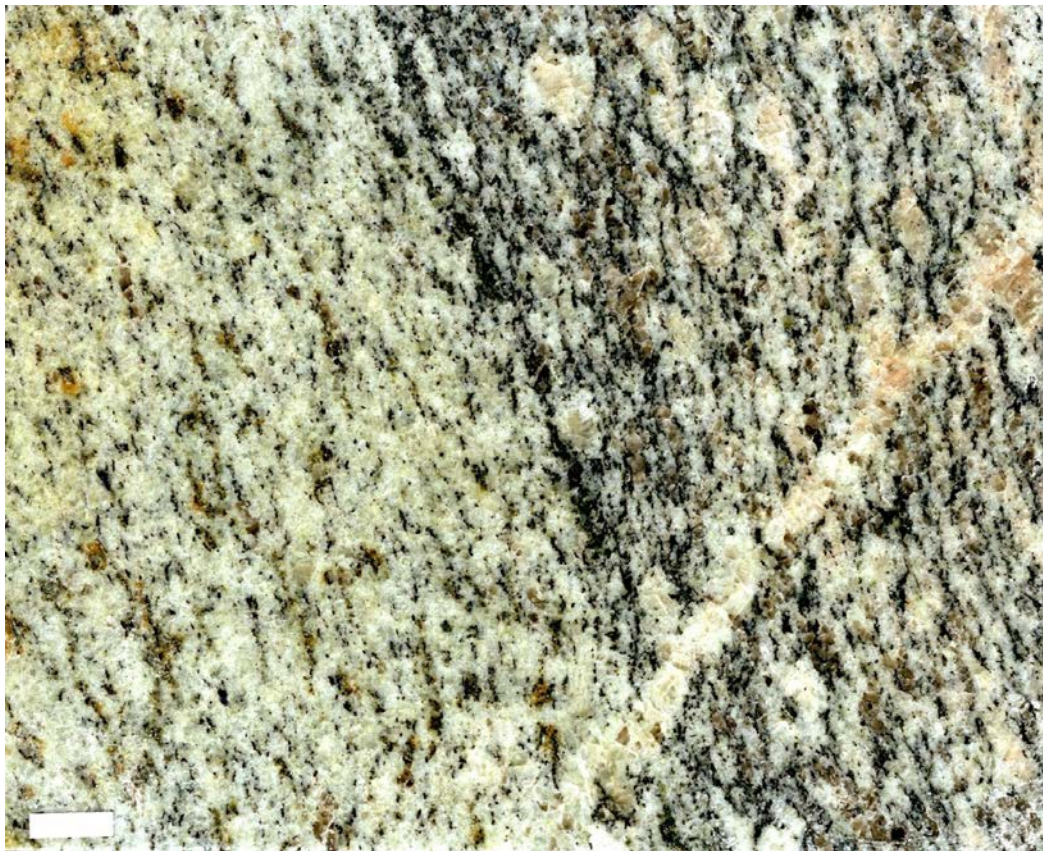


Figure 4. Hand specimen showing the contact between porphyritic reddish biotite granite (right) and mineralized, grey quartz-rich granite (left) from the Ørnehommen mine, upper tunnel (sample 25091306). The scale corresponds to 1 cm.

4. Description of macroscopic mineralization styles

4.1 Kvina mine

The Kvina mine is situated in a foliation-concordant, ca. 30° E-dipping pegmatite sheet which is up to 5 m thick and extends approximately 300 m in N-S direction and 150 m in E-W direction. It is the only mine in a large-scale mineralized pegmatite. The pegmatite shows strong internal ductile deformation. The reddish porphyritic granite close to the lower and upper contacts with the pegmatite is more intensively foliated than away from the contacts (Figure 5). The pegmatite contains nests of coarse-grained molybdenite commonly associated with megacrystic but re-crystallized biotite and along pegmatite-internal shear planes (Figures 6, 7). In addition, coarse-grained molybdenite occurs randomly in megacrystic pegmatite quartz and K-feldspar. Mineralized, foliation-concordant pegmatitic quartz bands (up to 20 cm wide and several meters long) are found in the reddish porphyritic granite beneath the major pegmatite. The entire sequence is cross-cut by sub-vertical, undeformed, non-mineralized pegmatite dykes (up to 0.5 m wide and several meters long).

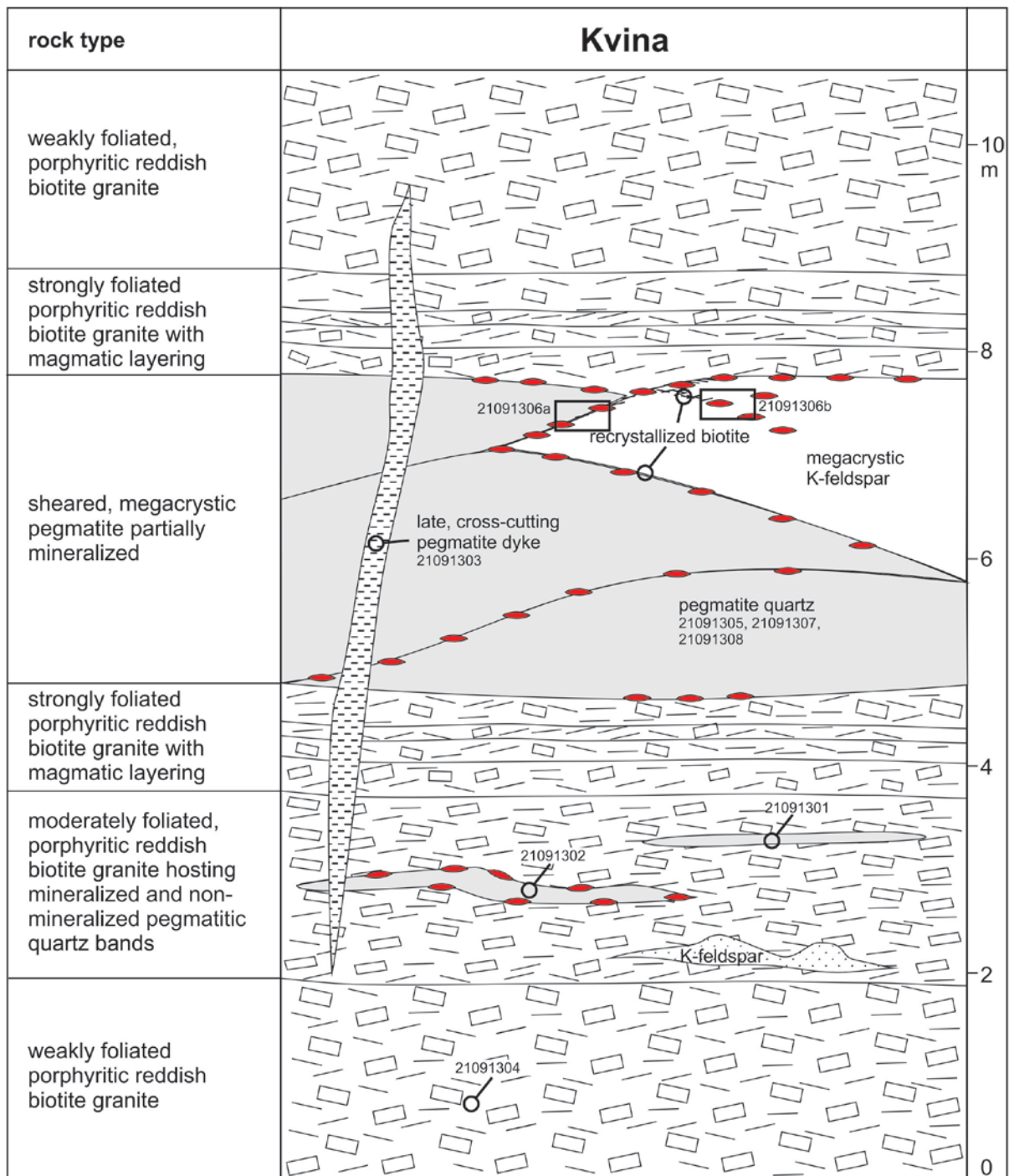


Figure 5. Simplified scheme of lithologies and mineralization styles exposed in the Kvina mine. The red disks indicate the location of coarse-grained molybdenite mineralization. The numbers correspond to sample numbers (see also Appendix 1).

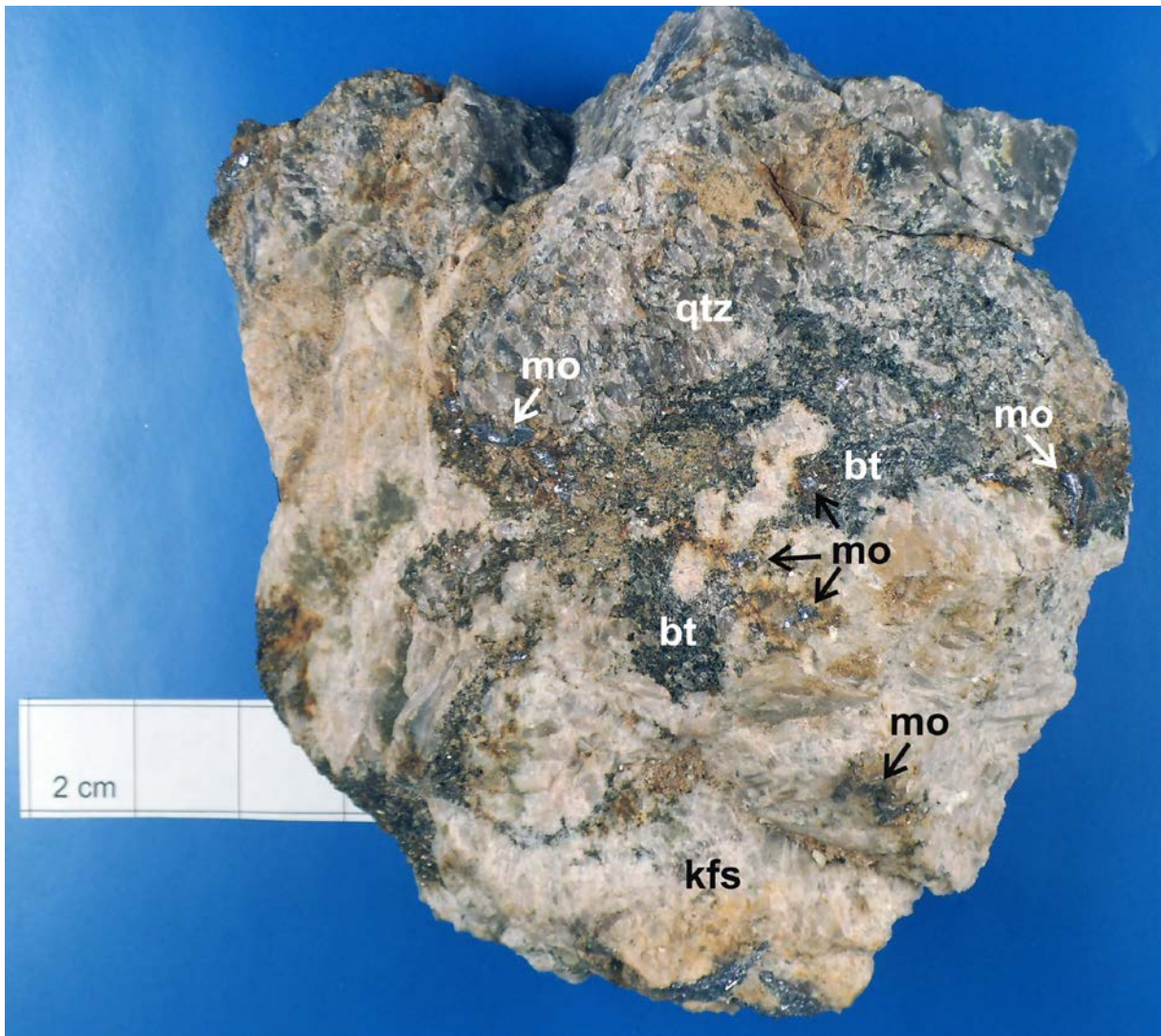


Figure 6. Hand specimen of deformed and mineralized pegmatite from the Kvina mine (sample 21091306a). *bt* – biotite, *kfs* – K-feldspar, *mo* – molybdenite, *qtz* - quartz.

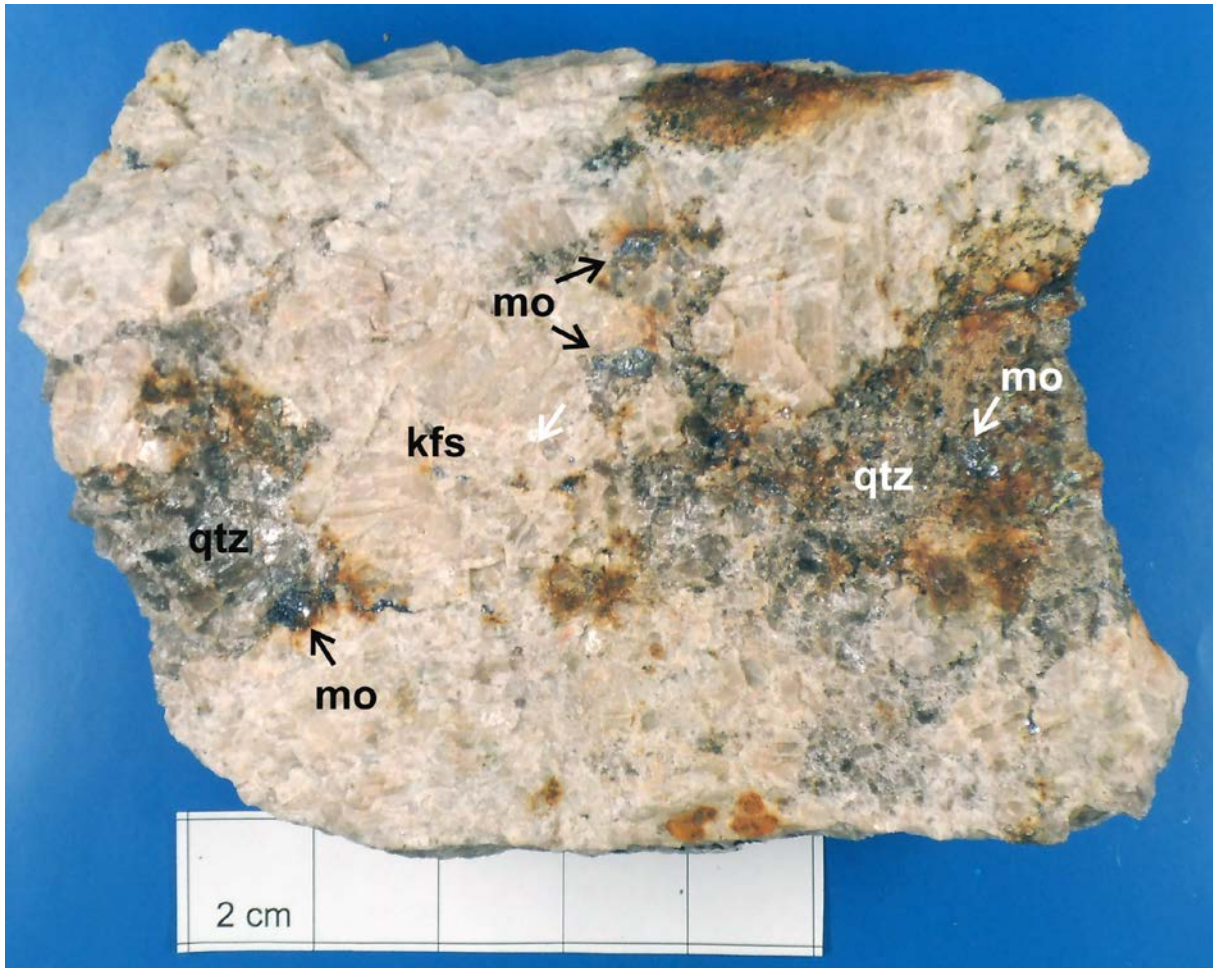


Figure 7. Hand specimen of deformed and mineralized pegmatite from the Kvina mine (sample 21091306b). *kfs* – K-feldspar, *mo* – molybdenite, *qtz* - quartz.

4.2 Knaben 1 mine

The characteristic features of the Knaben 1 mine are meter-scale xenoliths of amphibolite (at least 2 m thick and several decameters in sub-horizontal extension) and flaser gneiss (>5 m thick and several decameters in sub-horizontal extension). The coarse-grained molybdenite mineralization is bound to sub-horizontal pegmatitic quartz bands (0.5 to 20 cm thick, several meters in lateral extension) hosted by flaser gneiss (Figure 8). Occasionally the quartz bands grade into aplitic feldspar bands with coarse-grained molybdenite (Figure 9). The quartz bands cross-cut the foliation of the flaser gneiss with low angle of 5 to 10°. Boudinaged, zoned dykes of dioritic(?) composition occur in the northern part of the mine together with an up to 1 m wide sub-vertical, undeformed, non-mineralized pegmatite dyke.

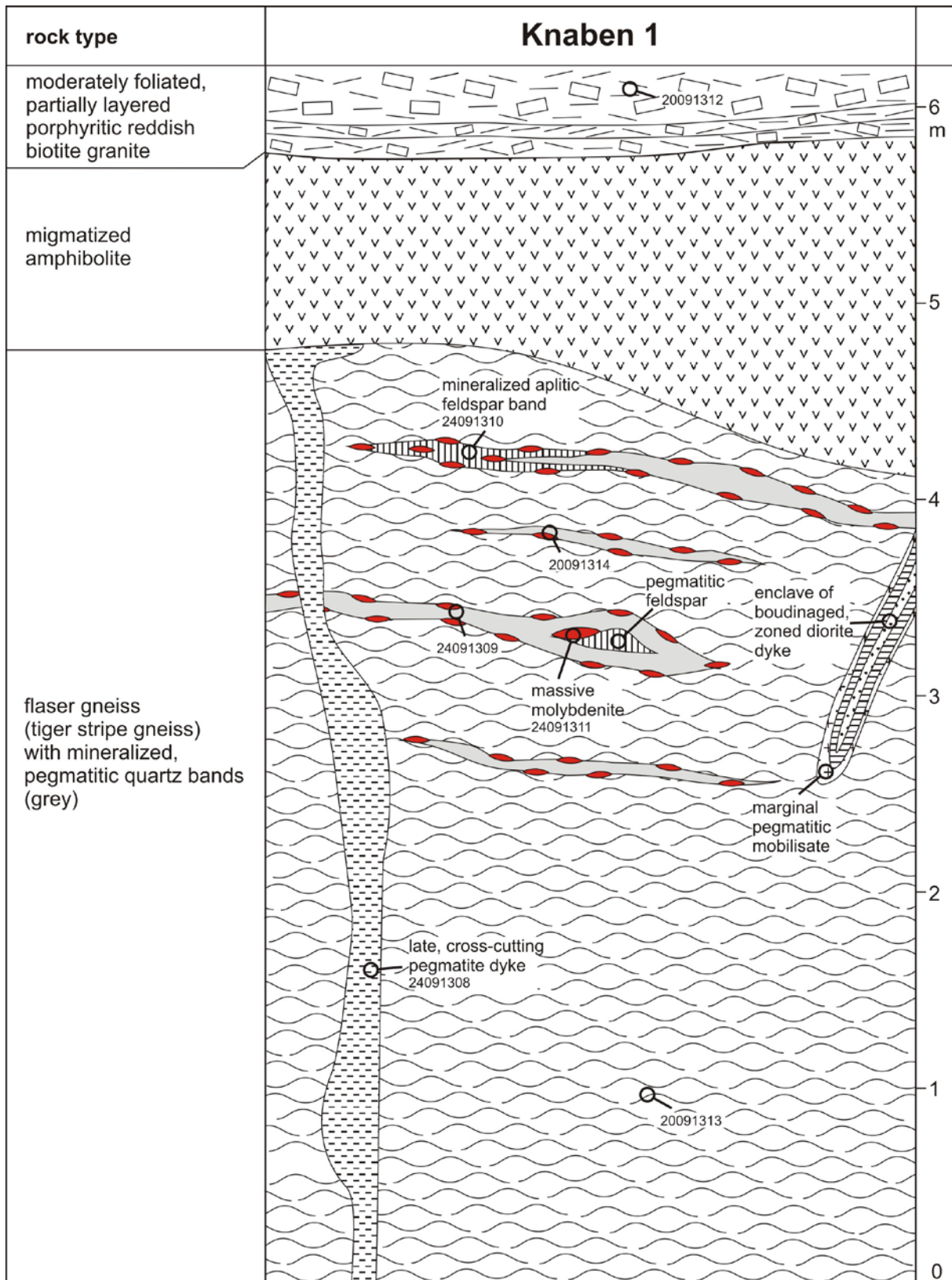


Figure 8. Simplified scheme of lithologies and mineralization styles exposed in the Knaben 1 mine. The late, cross-cutting pegmatite stopped during emplacement at the contact between flaser gneiss and amphibolite due to the lithological contrasts and not because it was “cut” by the amphibolite. The red disks indicate the location of coarse-grained molybdenite mineralization. The numbers correspond to sample numbers (see also Appendix 1).



Figure 9. Hand specimen of an aplitic feldspar vein with coarse-grained molybdenite (sample 24091310).

4.3 Synnøve 3 mine

The Synnøve 3 mine is a short (ca. 10 m long) U-shaped tunnel with entrances at both ends. Coarse-grained molybdenite mineralization is bound to a up to 5 cm thick pegmatitic quartz band (Figure 10). The slightly discordant (5 to 10° to the foliation) quartz band is embedded in flaser gneiss. Some minor fine-grained molybdenite occurs disseminated in the flaser gneiss.

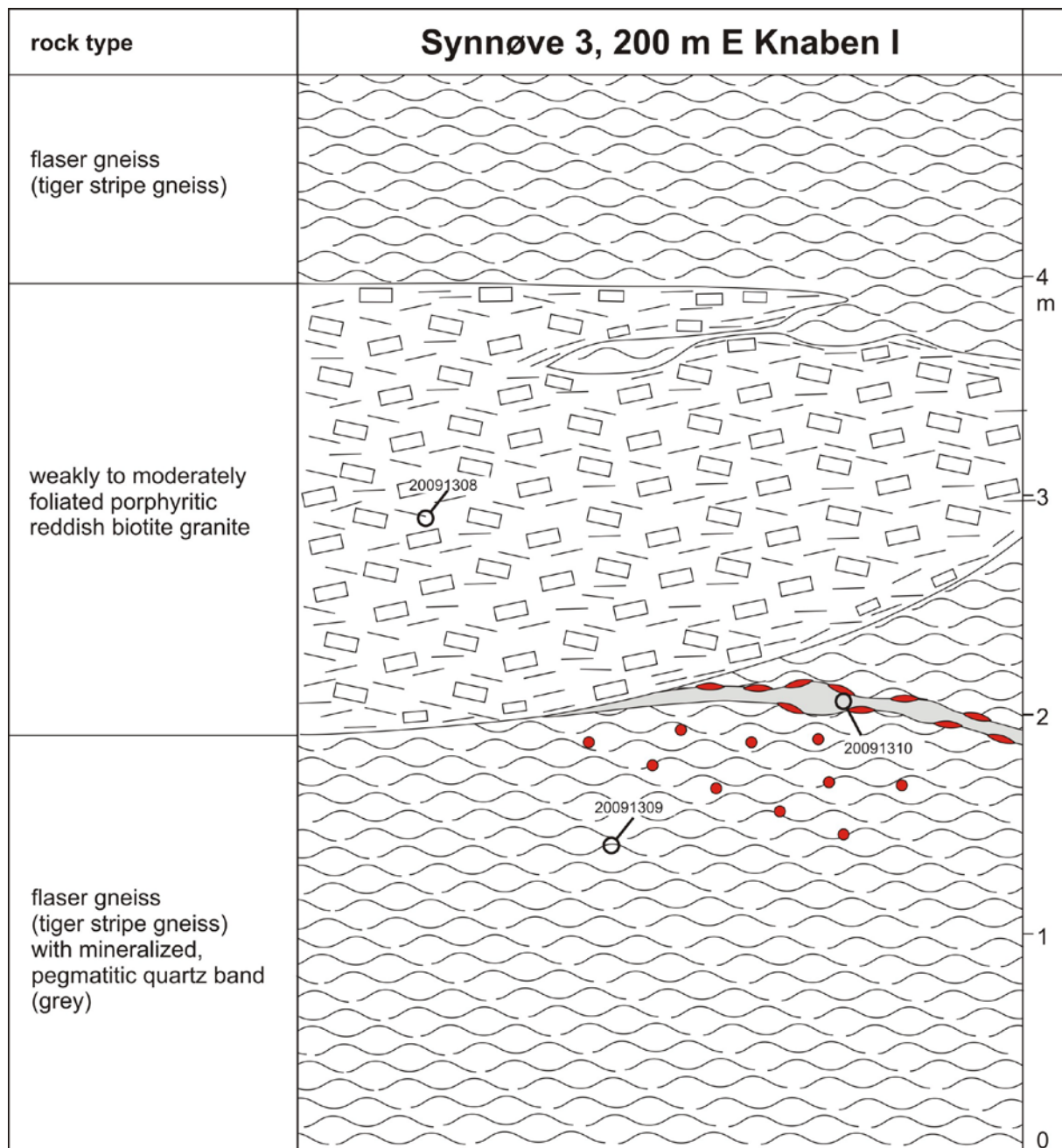


Figure 10. Simplified scheme of lithologies and mineralization styles exposed in the Synnøve 3 mine. The red disks indicate the location of coarse-grained molybdenite mineralization and the red dots that of fine-grained, disseminated molybdenite mineralization. The numbers correspond to sample numbers (see also Appendix 1).

4.4 Spillebrok-skjærpene, east tunnel

Flaser gneiss containing mineralized, pegmatitic quartz bands (up to 5 cm thick and several meters long) is exposed in the eastern tunnel of the Spillebrok-skjærpene (Figure 11). Foliation-concordant xenoliths of amphibolite (up to 20 cm thick and several meters long) occur within and at contacts of the flaser gneiss. The amphibolites are partially migmatized.

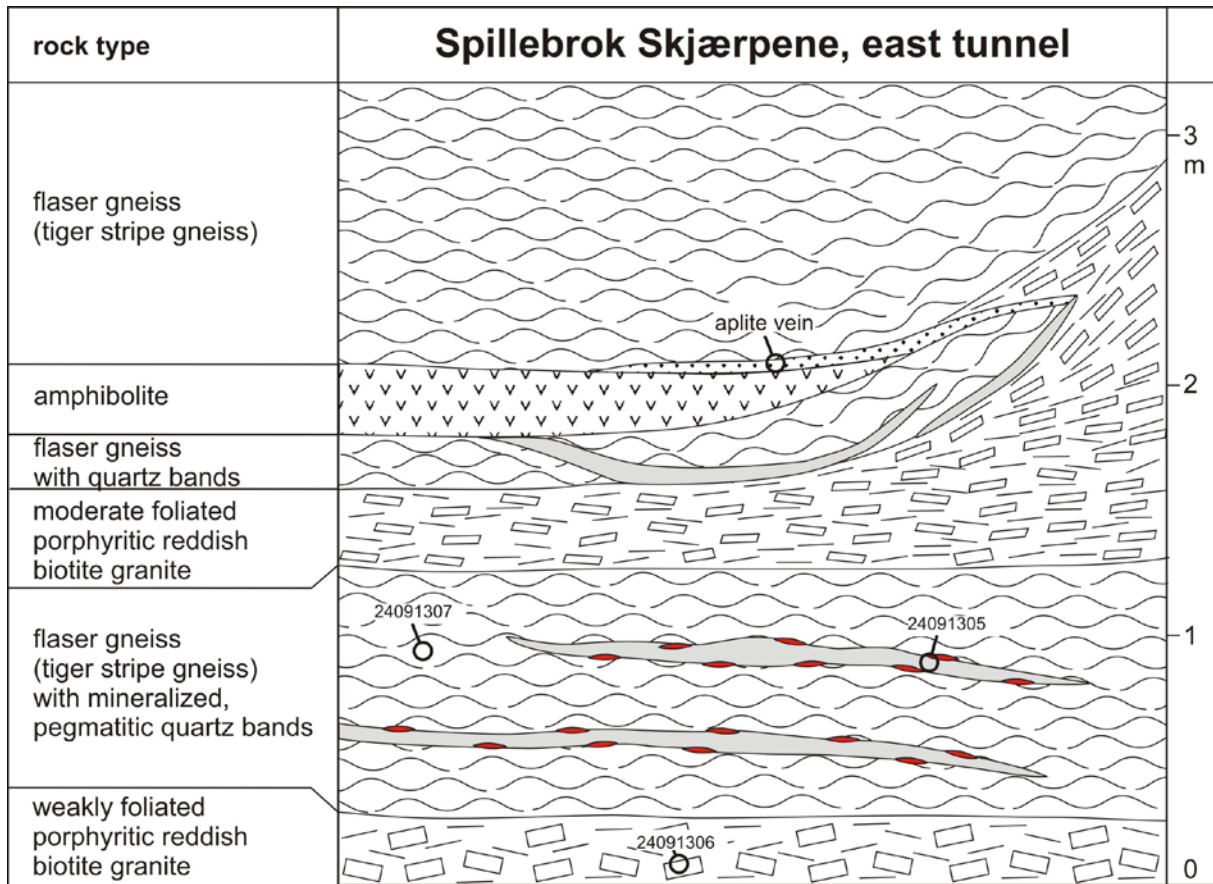


Figure 11. Simplified scheme of lithologies and mineralization styles exposed in the eastern tunnel of the Spillebrok-skjærpene. The red disks indicate the location of coarse-grained molybdenite mineralization related to pegmatitic quartz bands. The numbers correspond to sample numbers (see also Appendix 1).

4.5 Roma mine, upper north tunnel

In the upper north tunnel of the Roma mine the molybdenite mineralization is bond to pegmatitic quartz bands (up to 5 cm thick and several meters long) (Figure 12). The quartz bands occur in flaser gneiss. The reddish porphyritic granite exposed below the flaser gneiss contains a mega enclave (>10x10x5 m) of dark, biotite-rich granite of presumably granodioritic composition (Figure 13). The contact between the granites is diffuse and foliation-parallel. It is the only mine in which such a type of enclave has been observed. The dip of the main crystallization foliation varies significantly within the mine.

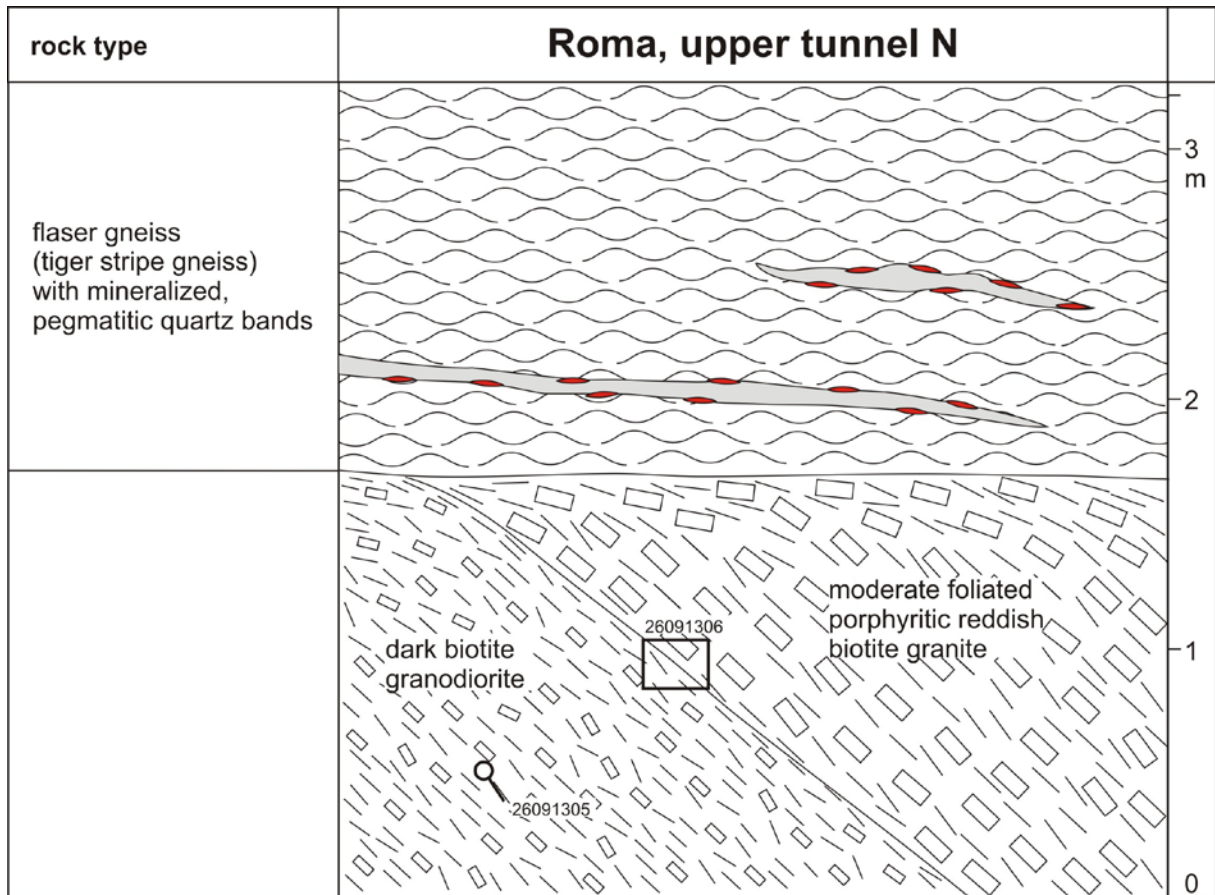


Figure 12. Simplified scheme of lithologies and mineralization styles exposed in the Roma mine, upper north tunnel. The red disks indicate the location of coarse-grained molybdenite mineralization related to pegmatitic quartz bands. The numbers correspond to sample numbers (see also Appendix 1).



Figure 13. Hand specimen showing the diffuse contact between reddish porphyritic granite (upper right) and biotite-rich granite of presumably granodioritic composition (sample 26091306). The scale corresponds to 1 cm.

4.6 Roma mine, upper south tunnel

In the upper south tunnel of the Roma mine coarse-grained molybdenite mineralization occurs at the upper and lower contacts of pegmatitic quartz bands which are up to 20 cm thick and several meters long (Figure 14). The common occurrence of large xenoliths of amphibolites is typically for the mine. They appear commonly at the upper part of the flaser gneiss section. It is the only mine where mineralized pegmatitic quartz bands have been observed within amphibolite mega enclaves. Late, undeformed, non-mineralized, K-feldspar-rich pegmatites crosscut the entire sequence perpendicular to the foliation but also sub-parallel to the foliation (Figure 15).

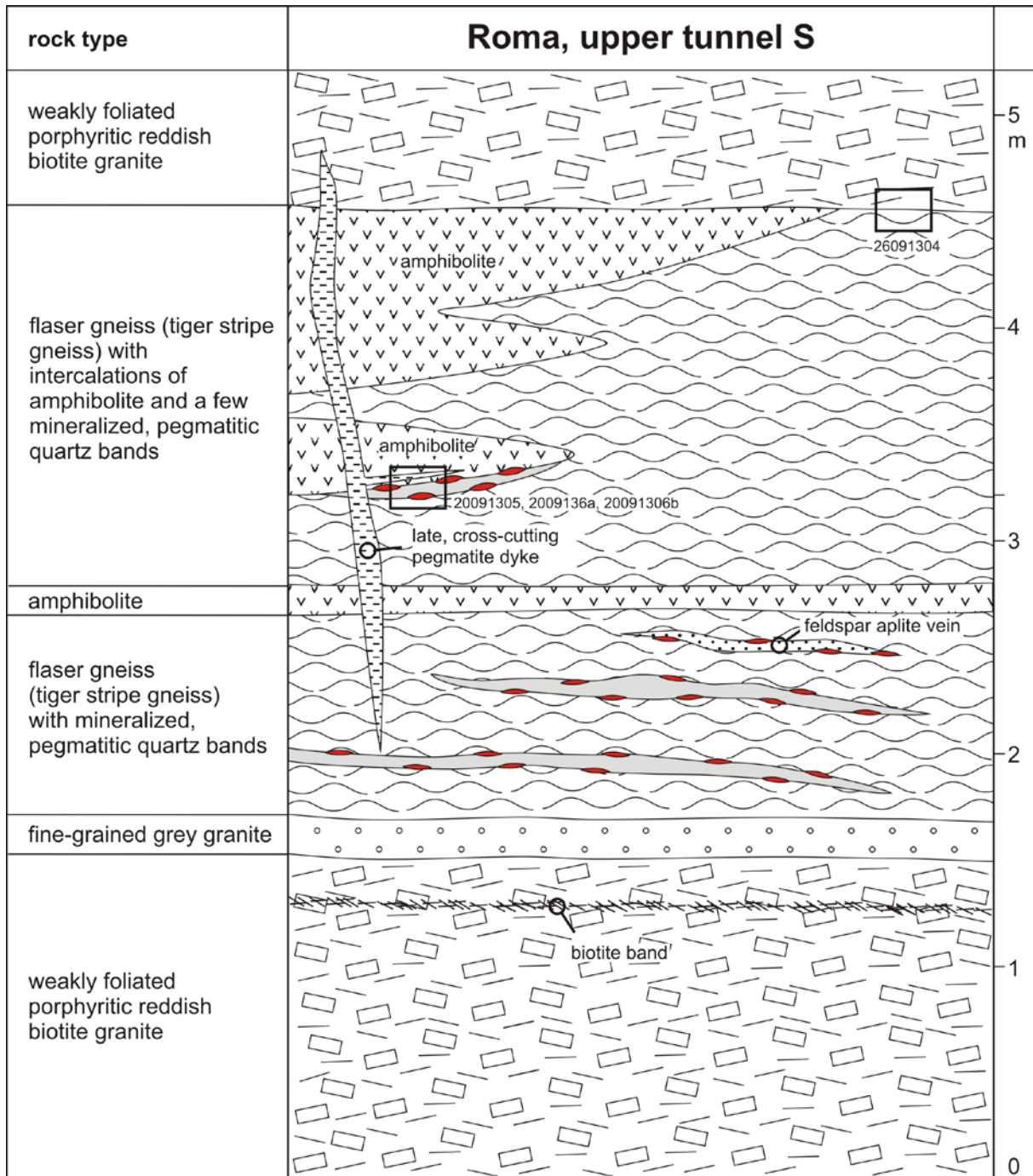


Figure 14. Simplified scheme of lithologies and mineralization styles exposed in the Roma mine, upper south tunnel. The red disks indicate the location of coarse-grained molybdenite mineralization related to pegmatitic quartz bands. The numbers correspond to sample numbers (see also Appendix 1).

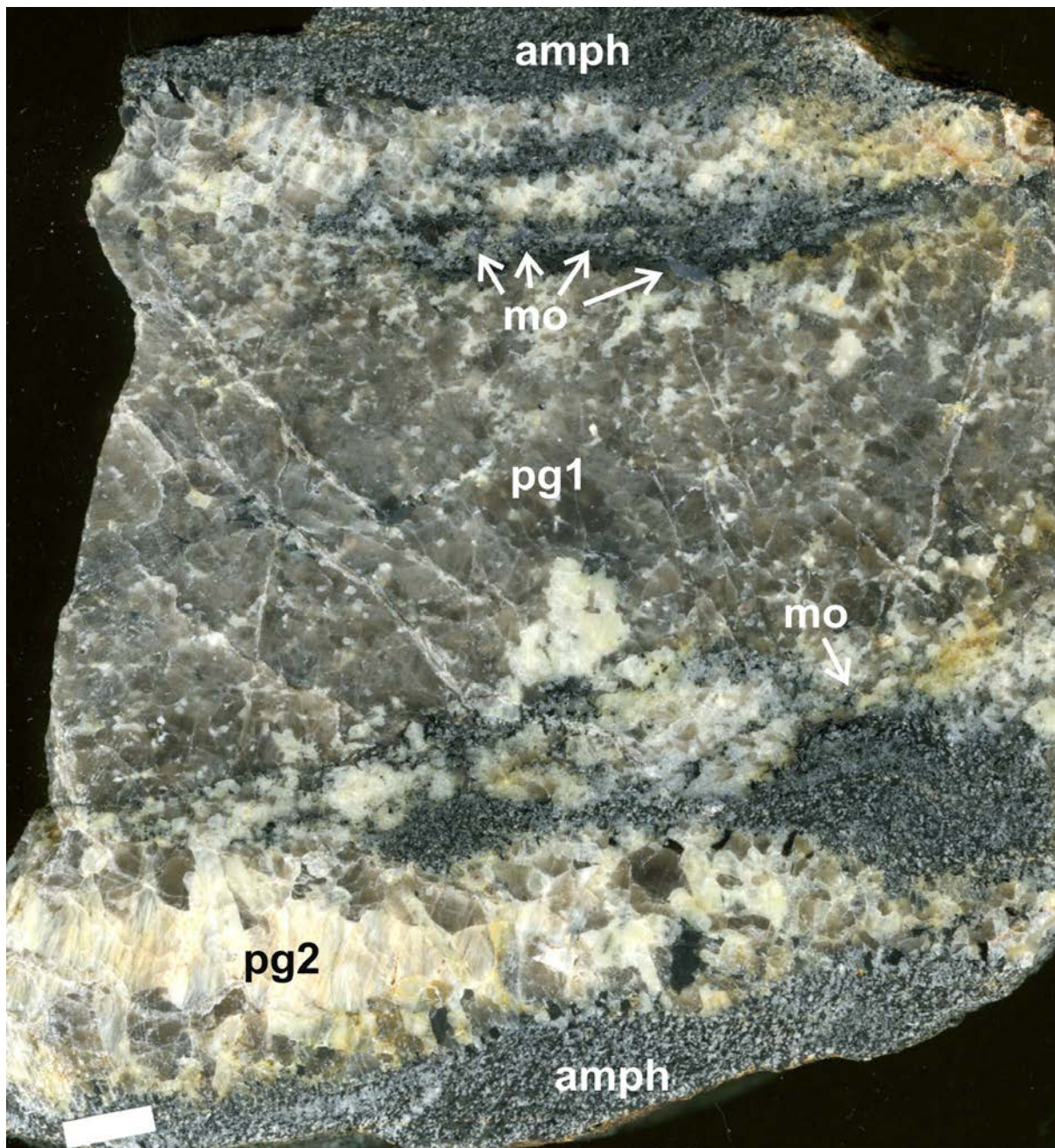


Figure 15. Hand specimen showing a pegmatitic quartz band (pg1) with coarse-grained molybdenite mineralization (mo) at the upper and lower contact (sample 20091306b). The quartz band occurs in migmatized amphibolite (amph). A late, undeformed, non-mineralized, K-feldspar-rich pegmatite vein (pg2) crosscut with low angle the foliation of the amphibolite and quartz band. The scale corresponds to 1 cm.

4.7 Roma mine, lower tunnel “Grundstollen”

In the “Grundstollen” the major part of the coarse-grained molybdenite mineralization is associated with a up to 30 cm thick pegmatitic, ductile sheared quartz band (Figure 16). The quartz band is located at the lower contact of a flaser gneiss mega xenolith (about 4 m thick) to the reddish porphyritic granite. Smaller mineralized quartz bands occur within the flaser gneiss. Amphibolite xenoliths are commonly found at the upper and lower contacts of the c. 2 m thick flaser gneiss sheet. The sequence is cross-cut by steeply dipping, brittle fractures healed with hydrothermal quartz.

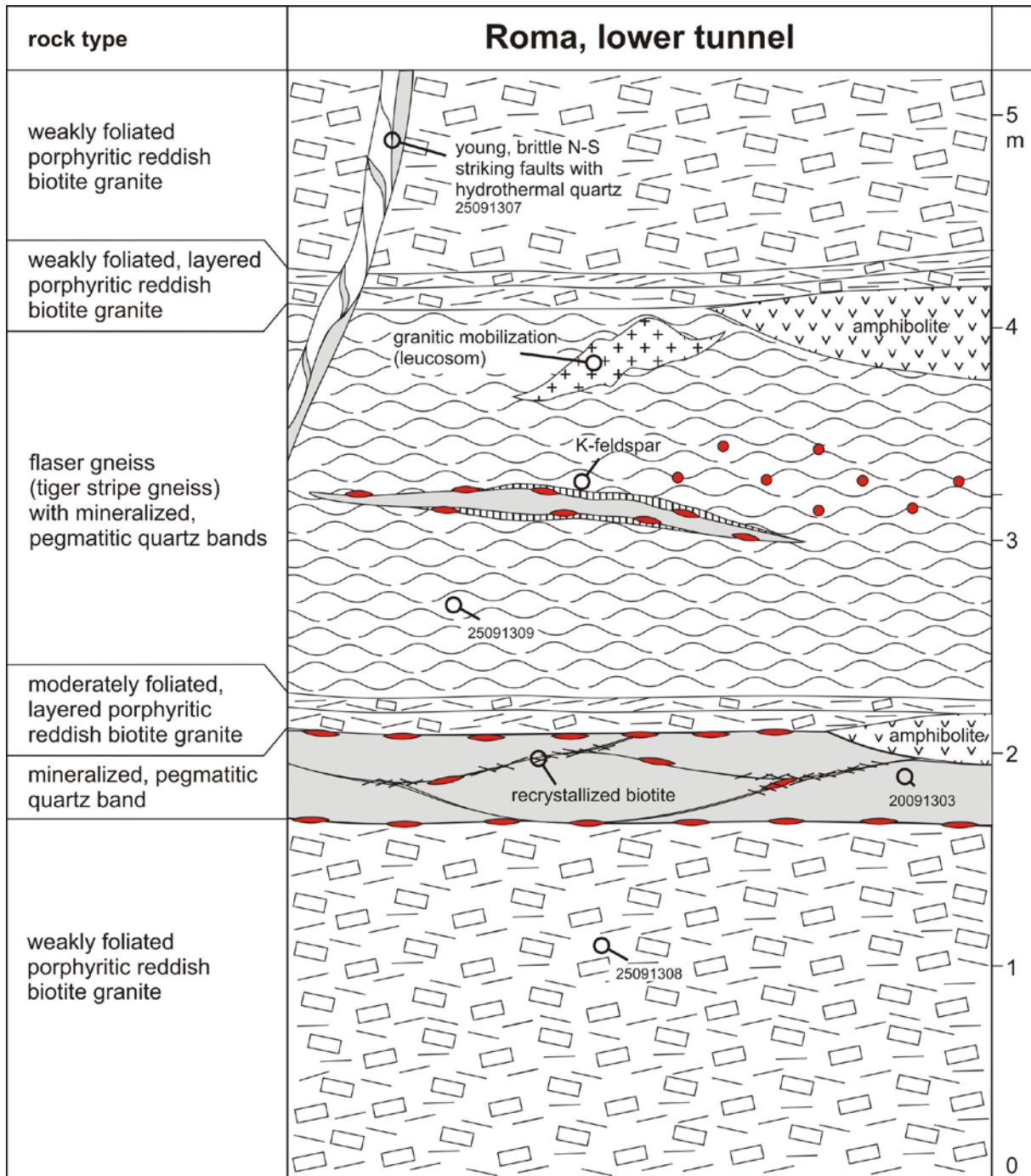


Figure 16. Simplified scheme of lithologies and mineralization styles exposed in the Roma mine, lower tunnel. The red disks indicate the location of coarse-grained molybdenite mineralization related to pegmatitic quartz bands and the red dots that of fine-grained, disseminated molybdenite. The numbers correspond to sample numbers (see also Appendix I).

4.8 Ørnehommen mine

The Ørnehommen mine is one of the larger mines in the Knaben mining district and extends over several levels. Coarse-grained molybdenite mineralization occurs in thin (<5 cm) pegmatitic quartz bands embedded in a ca. 50 cm thick sheet of moderately foliated porphyritic granite (Figure 17). A sheet of ca. 1 m thick, grey quartz-rich granite with fine-grained disseminated molybdenite mineralization occurs below the reddish porphyritic granite. The grey granite represents the same type of grey quartz-rich granite which is exposed in the Knaben 2 mine. In addition, several textural varieties of fine-grained, non-mineralized biotite granite occur (Figure 18) together with a white, K-feldspar-rich alaskite. Based on field observations the latter is younger than the reddish porphyritic granite and the fine-grained granites.

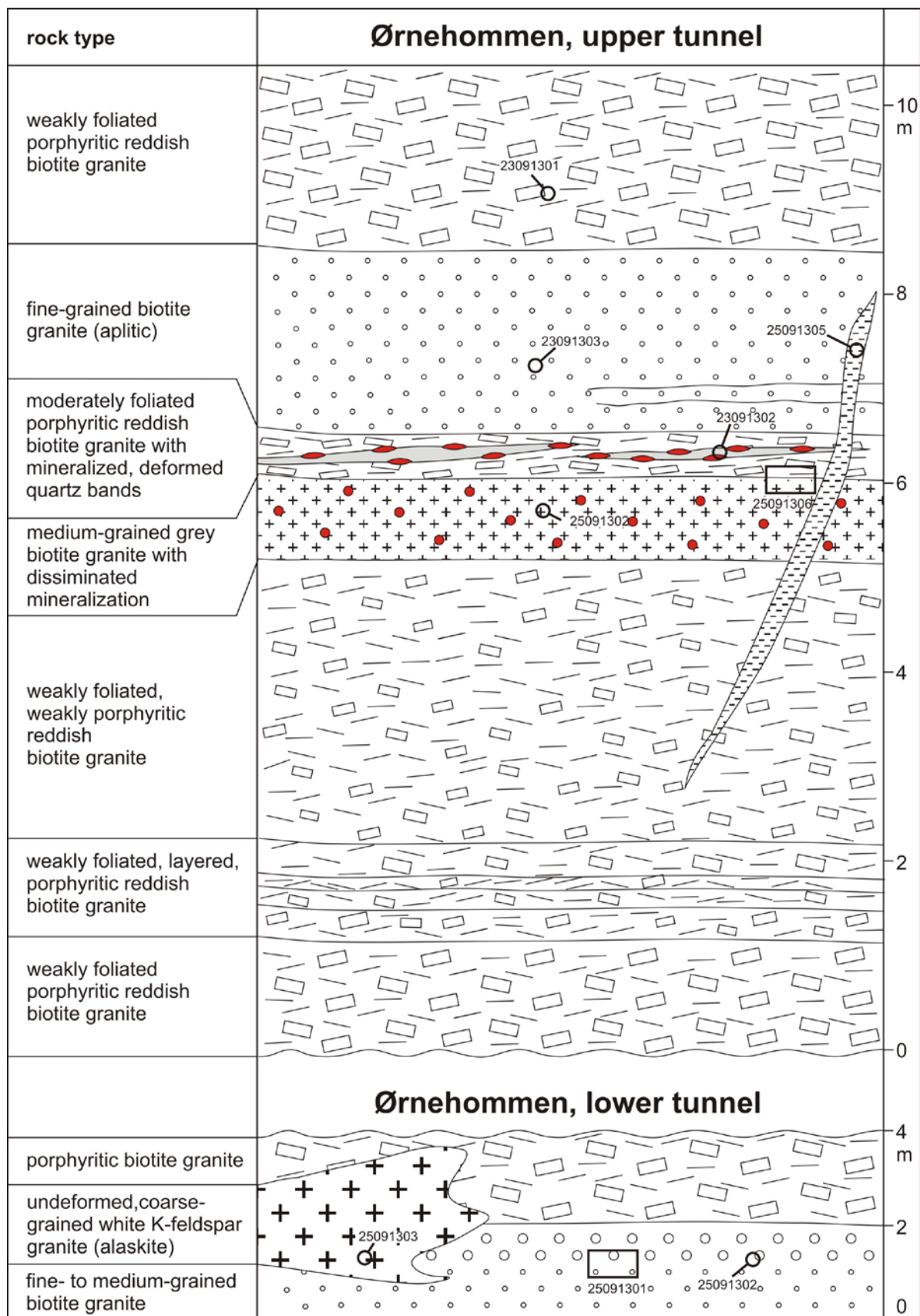


Figure 17. Simplified scheme of lithologies and mineralization styles exposed in the Ørnehommen mine. The red disks indicate the location of coarse-grained molybdenite mineralization related to pegmatitic quartz bands and the red dots that of fine-grained, disseminated molybdenite. The numbers correspond to sample numbers (see also Appendix 1).



Figure 18. Hand specimen showing the diffuse contact between non-mineralized, fine-grained and medium-grained, weakly porphyritic reddish biotite granite. Ørnehommen lower tunnel, sample 25091301. The scale corresponds to 1 cm.

4.9 Jelå mine, upper tunnel

In the Jelå mine upper tunnel the molybdenite mineralization occurs in up to 10 cm thick pegmatitic quartz bands hosted by moderately foliated reddish porphyritic granite (Figure 19). Some of the quartz bands are macroscopically free of molybdenite. The sequence is crosscut by a vertical, ca. 15 m wide meta-basalt dyke (“dolerite”).

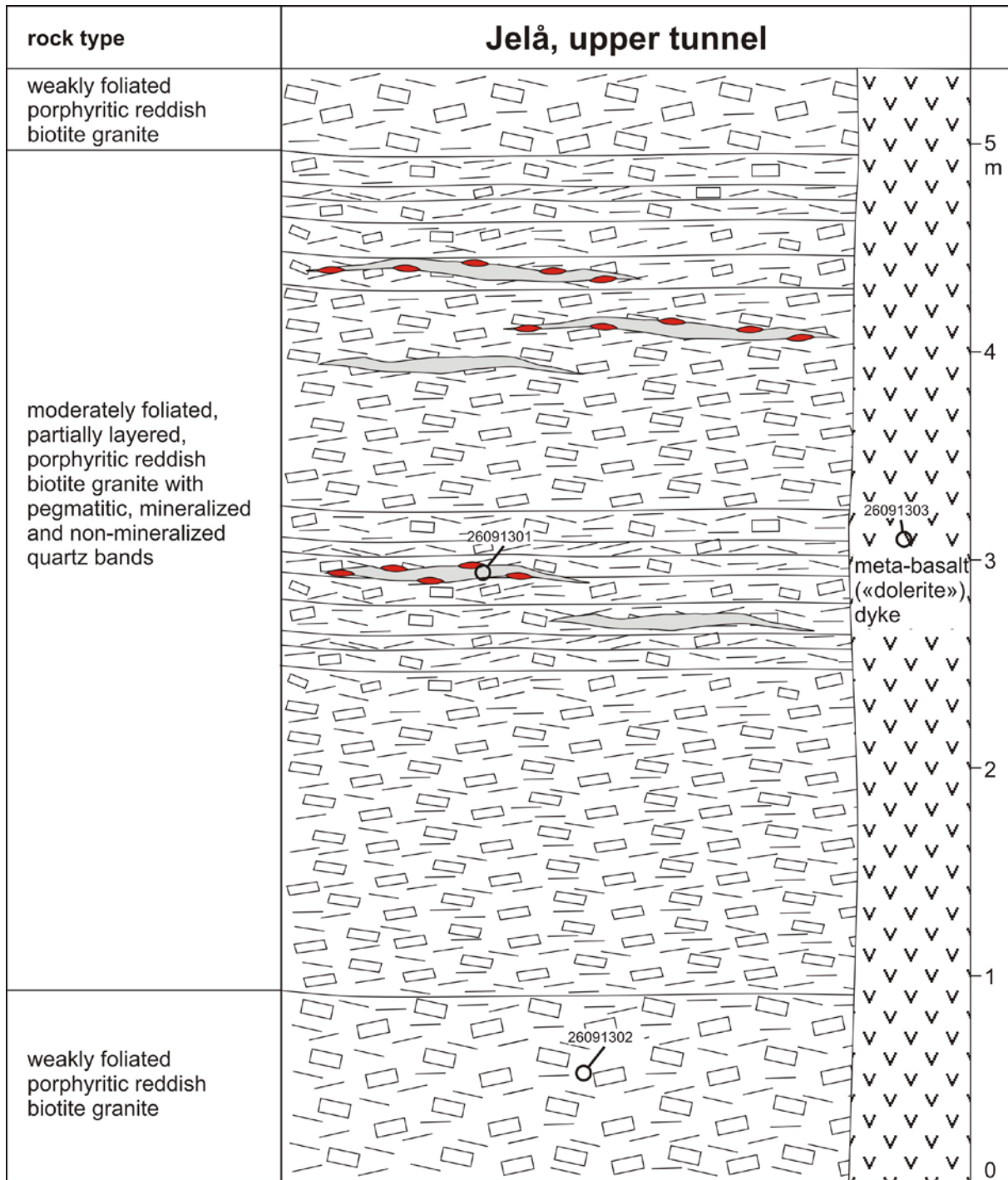


Figure 19. Simplified scheme of lithologies and mineralization styles exposed in the Jelå mine, upper tunnel. The red disks indicate the location of coarse-grained molybdenite mineralization related to pegmatitic quartz bands. The numbers correspond to sample numbers (see also Appendix 1).

4.10 Knaben 2 mine

The grey, quartz-rich granite is the main carrier of fine-grained, disseminated molybdenite in the Knaben 2 mine (Figure 20). The grey granite forms an up to 15 m thick, foliation-parallel sheet within porphyritic granite. It shows commonly a foliation-parallel layered structure due to heterogeneous distribution of rock-forming minerals and grain sizes. The grain size varies commonly between fine- to medium-grained, locally coarse-grained layers or batches occur (Figure 21). Pegmatitic quartz bands between 0.5 and 20 cm in thickness and with coarse-

grained molybdenite mineralization are common in the grey granite (Figure 22). The lower contact of the grey granite to the porphyritic granite is commonly marked by an up to 20 cm thick, mineralized pegmatitic quartz band. Some mineralized quartz bands occur also in the porphyritic granite. Occasionally, fine-grained disseminated molybdenite mineralization has been observed in the porphyritic granite close to the contact of the grey granite. In addition to the disseminated and quartz-band ore types, coarse-grained molybdenite occurs as fracture fillings within the grey granite (Figure 23). Non-mineralized, undeformed, foliation-parallel pegmatite sheets occur occasionally in the porphyritic granite. Late, brittle, sub-vertical, N-S-striking faults with chalcopyrite mineralization crosscut the sequence.

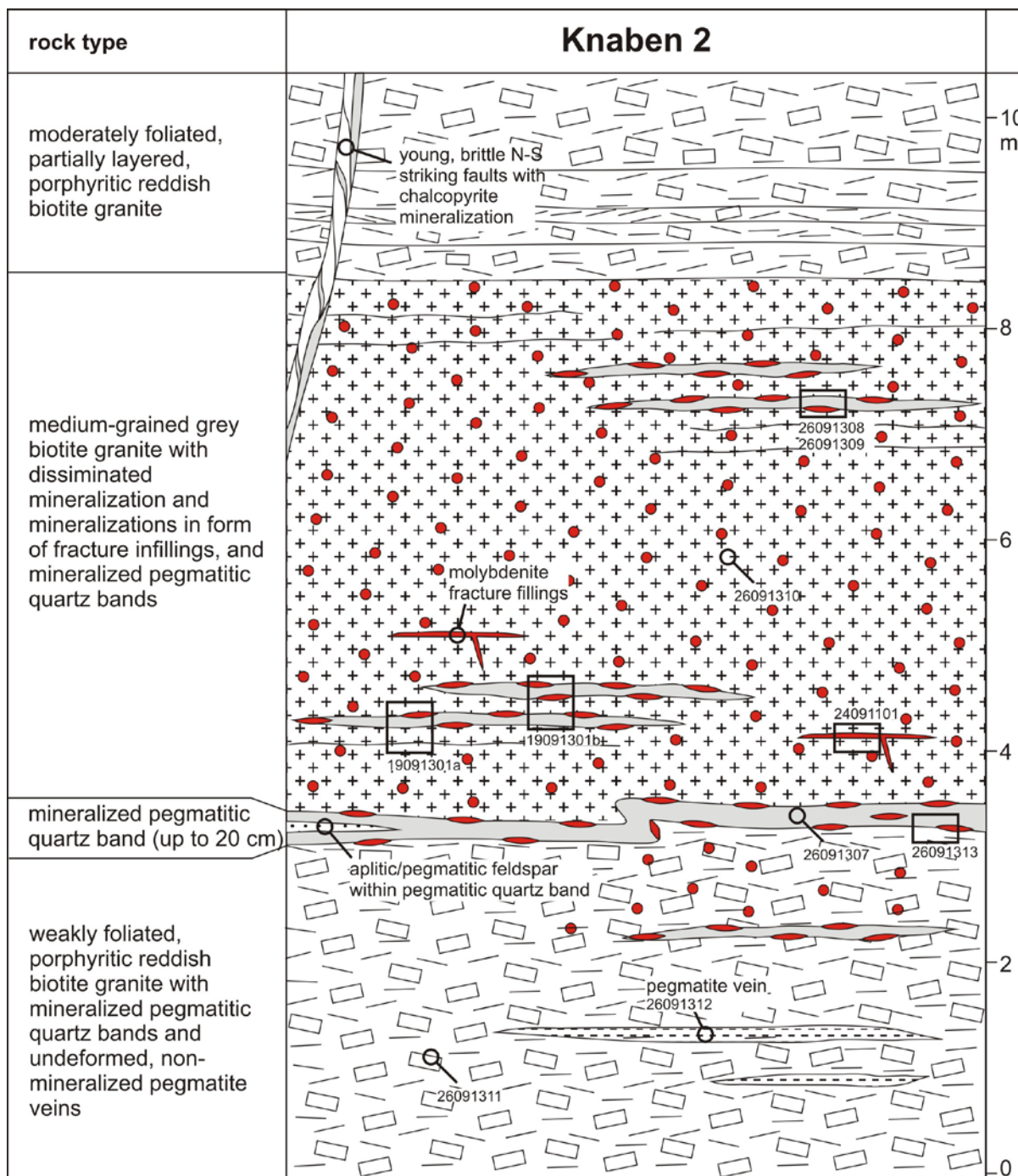


Figure 20. Simplified scheme of lithologies and mineralization styles exposed in the Knaben 2 mine. The red disks indicate the location of coarse-grained molybdenite mineralization related to pegmatitic quartz bands and the red dots that of fine-grained, disseminated molybdenite mineralization. The numbers correspond to sample numbers (see also Appendix I).

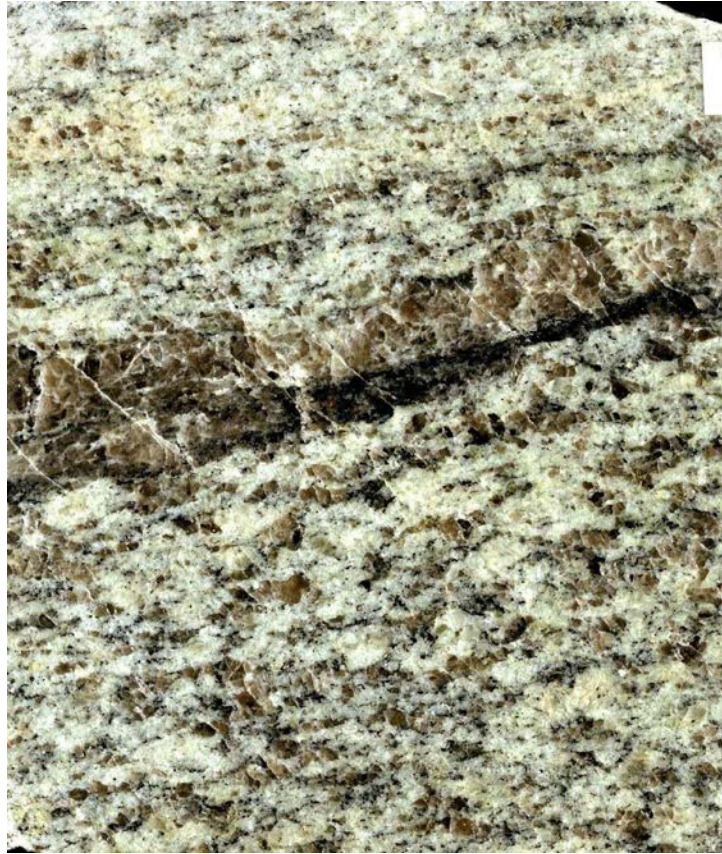


Figure 21. Hand specimen of grey, quartz-rich mineralized granite with changing grain size. The sample shows a foliation-concordant pegmatitic quartz band (center of image) with a biotite layer at the lower contact (sample 19091301a). The scale corresponds to 1 cm.

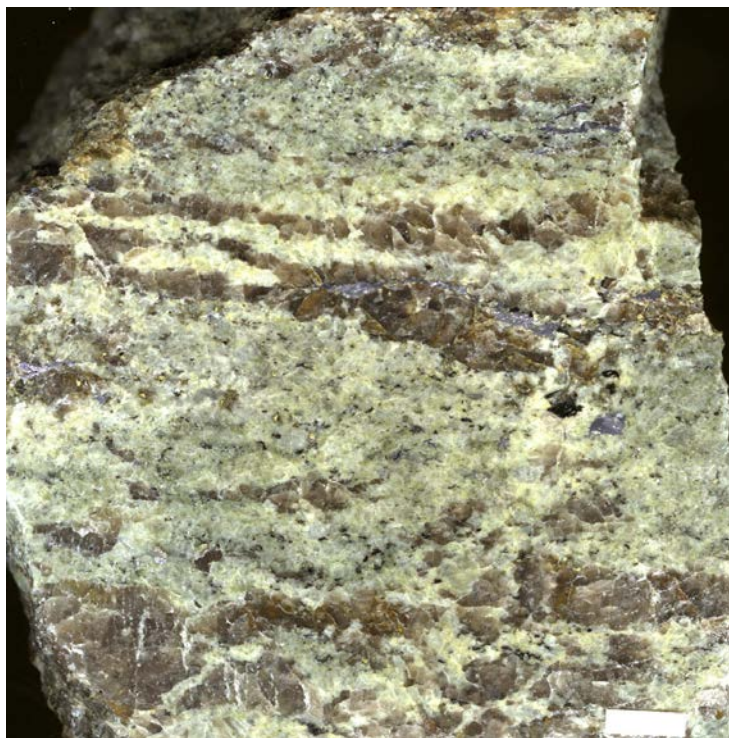


Figure 22. Hand specimen of grey, aplitic, mineralized granite interlayered with pegmatitic quartz bands with coarse-grained molybdenite (sample 19091301b). The scale corresponds to 1 cm.



Figure 23. Hand specimen of grey, quartz-rich granite with coarse-grained molybdenite fracture filling. Knaben 2 mine, sample 24091101. The edges of the squares on the scale corresponds to 2 cm.

4.11 Bragold mine

The molybdenite mineralization in the Bragold mine is related to up to 20 cm thick pegmatitic quartz bands (Figure 24). The quartz bands contain recrystallized pegmatitic feldspar and biotite. The host rock is weakly porphyritic, reddish granite and the degree of foliation increases in the vicinity of the quartz bands.

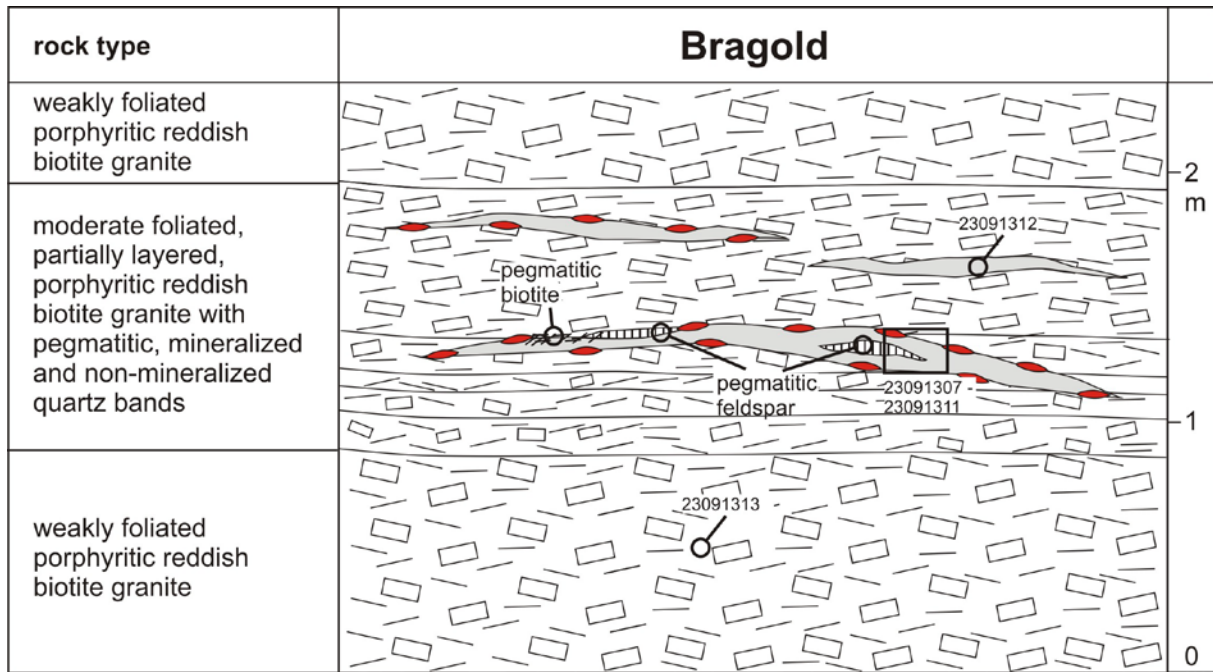


Figure 24. Simplified scheme of lithologies and mineralization styles exposed in the Bragold mine. The red disks indicate the location of coarse-grained molybdenite mineralization related to pegmatitic quartz bands. The numbers correspond to sample numbers (see also Appendix 1).

4.12 Hommen mine

The Hommen mine is a very small mine with a 8 m-long tunnel. Several stockpiles of mined ore occur near the tunnel entrance. Coarse-grained molybdenite mineralization is related to pegmatitic quartz bands (Figure 25). The quartz bands are brittle deformed in addition to the common ductile deformation. The brittle deformation is a specific feature of this mine. Weakly to moderately porphyritic reddish granite comprises the only host rock lithology within the mine. Some fine-grained disseminated molybdenite occurs in moderately foliated porphyritic granite close to the mineralized quartz bands.

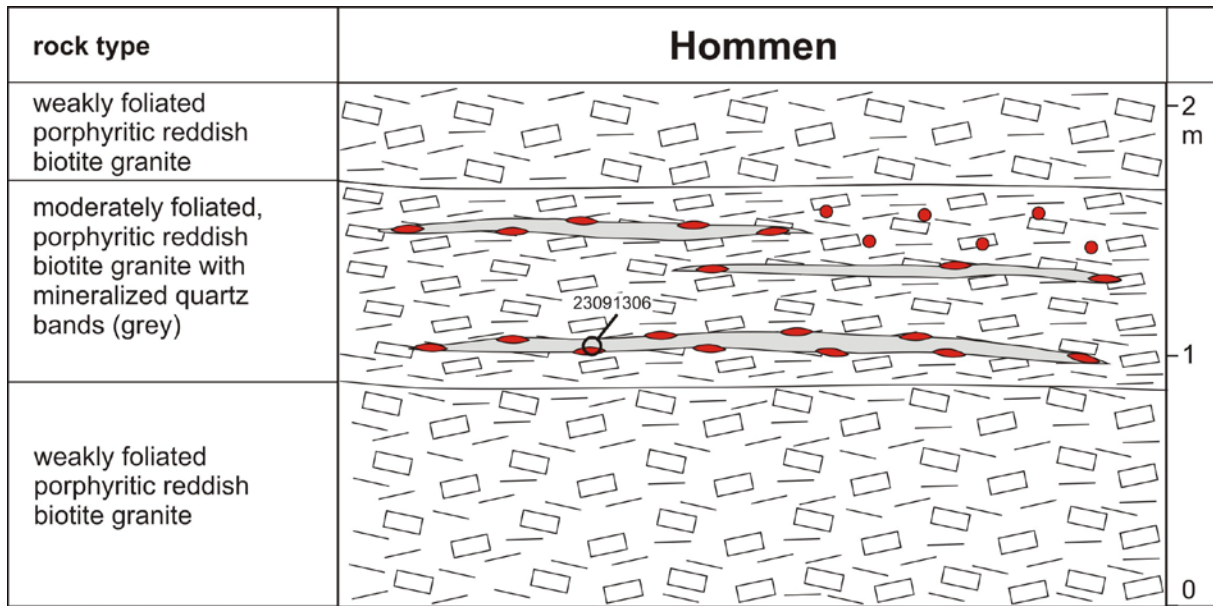


Figure 25. Simplified scheme of lithologies and mineralization styles exposed in the Hommen mine. The red disks indicate the location of coarse-grained molybdenite mineralization related to pegmatitic quartz bands and the red dots fine-grained disseminated molybdenite mineralization in moderately deformed porphyritic granite. The number corresponds to sample numbers (see also Appendix 1).

5. Summary of observed types of mineralization

Table 1 summarizes the structural types of molybdenite mineralization observed in the underground mines of the Knaben mining district. Principally two structural types of molybdenite mineralization are distinguished: (1) coarse-grained, concentrated molybdenite and (2) fine-grained, disseminated molybdenite. The latter is commonly associated with other (minor) sulfide minerals such as pyrite and chalcopyrite

An exceptional situation has been observed at the Hunsbedt Skjærp and Kopper Skjærp in the NE of the Knaben mining district. Here, the pegmatitic quartz bands containing coarse-grained molybdenite are superimposed by an intense chalcopyrite-chamosite-apatite mineralization (Figures 26, 27).

The macroscopically observed mineralization types have not been investigated at microscopic scale. This will be the task of future studies.

Table 1. Simplified classification of macroscopic observed structural styles of molybdenite mineralization in underground mines of the Knaben mining district.

type	sub-type	occurrence
coarse-grained concentrated molybdenite	in ductile deformed pegmatitic quartz bands, preferentially at the contacts of the quartz bands	all mines, most common mineralization type
	in aplitic feldspar veins which graduate from the pegmatitic quartz bands	Knaben 1, Roma upper south tunnel
	in large scale pegmatite	Kvina
	fracture fillings in the grey, quartz-rich granite	Knaben 2
	in ductile deformed pegmatitic quartz bands superimposed by chalcopyrite mineralization	Kopper Skjærp, Hunsbedt Skjærp
Fine-grained disseminated molybdenite	in grey, quartz-rich granite	Knaben 2, Ørnehommen
	in flaser gneiss mega xenoliths	Roma, upper south tunnel
	in reddish porphyritic granite	Knaben 2, Hommen

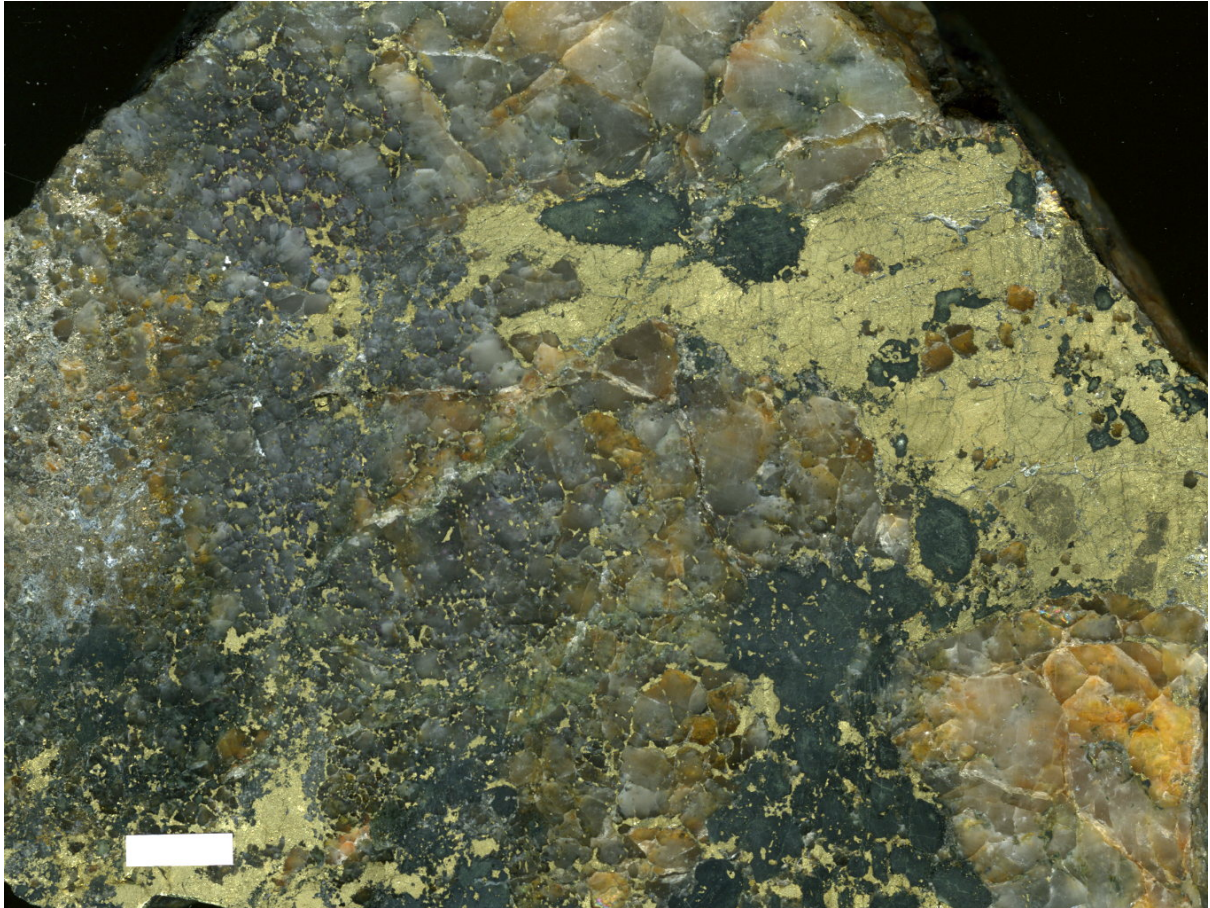


Figure 26. Hand specimen of pegmatitic quartz with minor molybdenite and massive chalcopyrite. Hunsbedt Skjærp, sample 20091317. The scale corresponds to 1 cm.

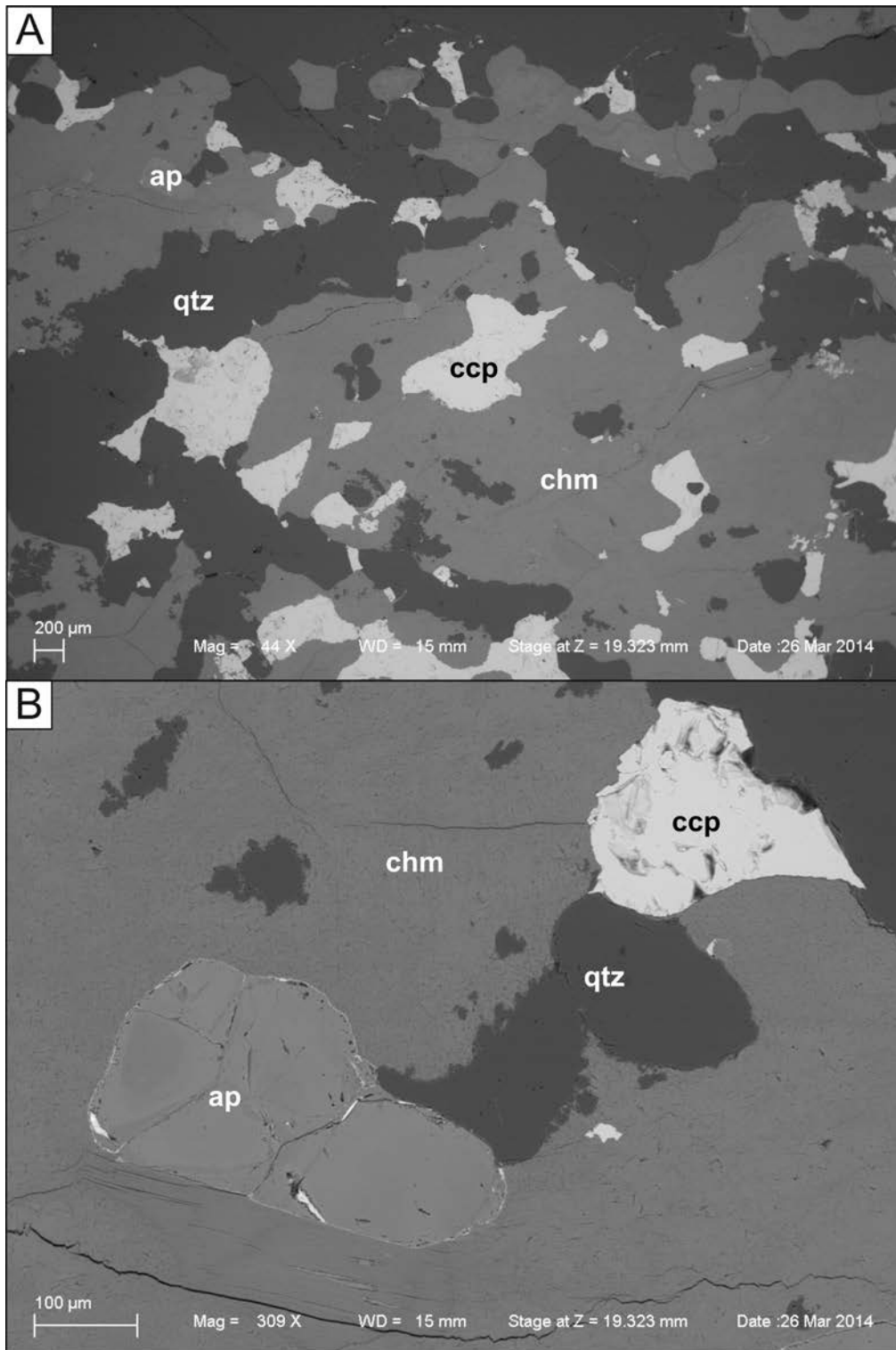


Figure 27. BSE images of the chalcopyrite-chamosite-apatite mineralization overprinting pegmatitic quartz bands with molybdenite mineralization. Hunsbedt Skjærp, sample 20091315. A – Overview image. B – Detailed image. Mineral abbreviations: ap – apatite, chm – chamosite, ccp - chalcopyrite.

6. Results

6.1 Cathodoluminescence-contrasted structures in quartz

Quartz of all investigated igneous rock types (reddish porphyritic granite, grey granite, flaser gneiss, pegmatitic quartz bands, undeformed pegmatites) has bright CL of high intensity (Figure 28). Only the hydrothermal quartz crystals of late, brittle faults exposed in the lower Roma mine exhibit dull luminescence and a distinct primary growth zoning (sample 25091307, Figure 29). The bright luminescent igneous quartz is superimposed by several generations of secondary quartz with lower CL signal. These secondary quartz generations are generally similar for all investigated igneous quartz samples. Most common are thin (<5 µm), non-luminescent, trans-granular healed fractures connecting non-luminescent domains around secondary fluid inclusions (sqtz 1, Figure 28). These structures appear black in the SEM-CL image and are characteristic for plutonic rocks in general (Müller et al. 2010 and references therein). In addition, non-luminescent quartz coatings occur along grain boundaries which sometimes can hardly be distinguished from the trans-granular fractures (sqtz 2; Figures 28D, E). Other common secondary structures are dull luminescent irregular domains with fracture-like patterns (dark grey in SEM-CL; sqtz 3). In some cases these structures seem to be related to the trans-granular fractures (Figure 28E) in other cases not (Figure 28D).

Oscillatory zoned growth fronts at crystal margins are the most distinctive structures detected in the Knaben samples (sqtz 4; Figure 30). The wavy, oscillatory zoning follows approximately the outline of the grain boundary. These growth fronts form tongues of dull luminescent quartz bulging into and replacing bright luminescent primary quartz (pqtz) by grain boundary migration (Figure 30). The grains exhibiting these structures have commonly a lower CL signal as the surrounding quartz crystals and less secondary structures which seem to be deleted partially, particularly sqz3. In some samples the replacement structures occupy up to 25 % of the quartz. Similar structures have been described from amphibolite facies quartzites, i.e. Tverrådalen, Nasafjellet and Melkfjellet in Norway (Müller et al. 2007, 2012). The structures are interpreted as solid-solution replacement structures were crystals with less defects (low CL intensity) replace crystals with higher defect abundance (high CL intensity). The textures developed post-magmatically during high temperatures which remained over a relative long period. Because this texture is omnipresent in all investigated igneous rocks, they indicate a regional thermal event, likely due to long-lasting heat flow and fluid circulation as a result of voluminous, long-lived (c. 1060 to 920 Ma) magmatism related to the Sirdal Magmatic Belt and Hornblende-Biotite Granite Suite (Slagstad et al. 2013; Coint et al. 2015).

The chalcopyrite (ccp)- chamosite (chm) – apatite (ap) mineralization at Hunsbedt and Kopper Skjærp is associated with quartz generation showing dull CL (sqtz5) (Figure 31). During this mineralization stage the quartz related to the molybdenite mineralization is replaced and new zoned sub-euhedral (sqtz5a) and dendritic quartz (sqtz5b) were formed.

Summarizing, the general abundance of the observed secondary structures in the investigated igneous quartz types (reddish porphyritic granite, grey granite, flaser gneiss, pegmatitic quartz bands, undeformed pegmatites) is relative low compared to other plutonic environments worldwide (e.g. Müller et al. 2010) indicating that the amount of circulating, late-magmatic fluids was relative limited. The visualized CL- structures allow the conclusion that no significant quartz deformation occurred under retrograde conditions. Thus, the igneous quartz was deformed predominantly during the syn-kinematic emplacement of the magmas and the foliation developed from the combination of magmatic and solid state flow. However, this statement should be confirmed by additional microscopic studies of the quartz texture.

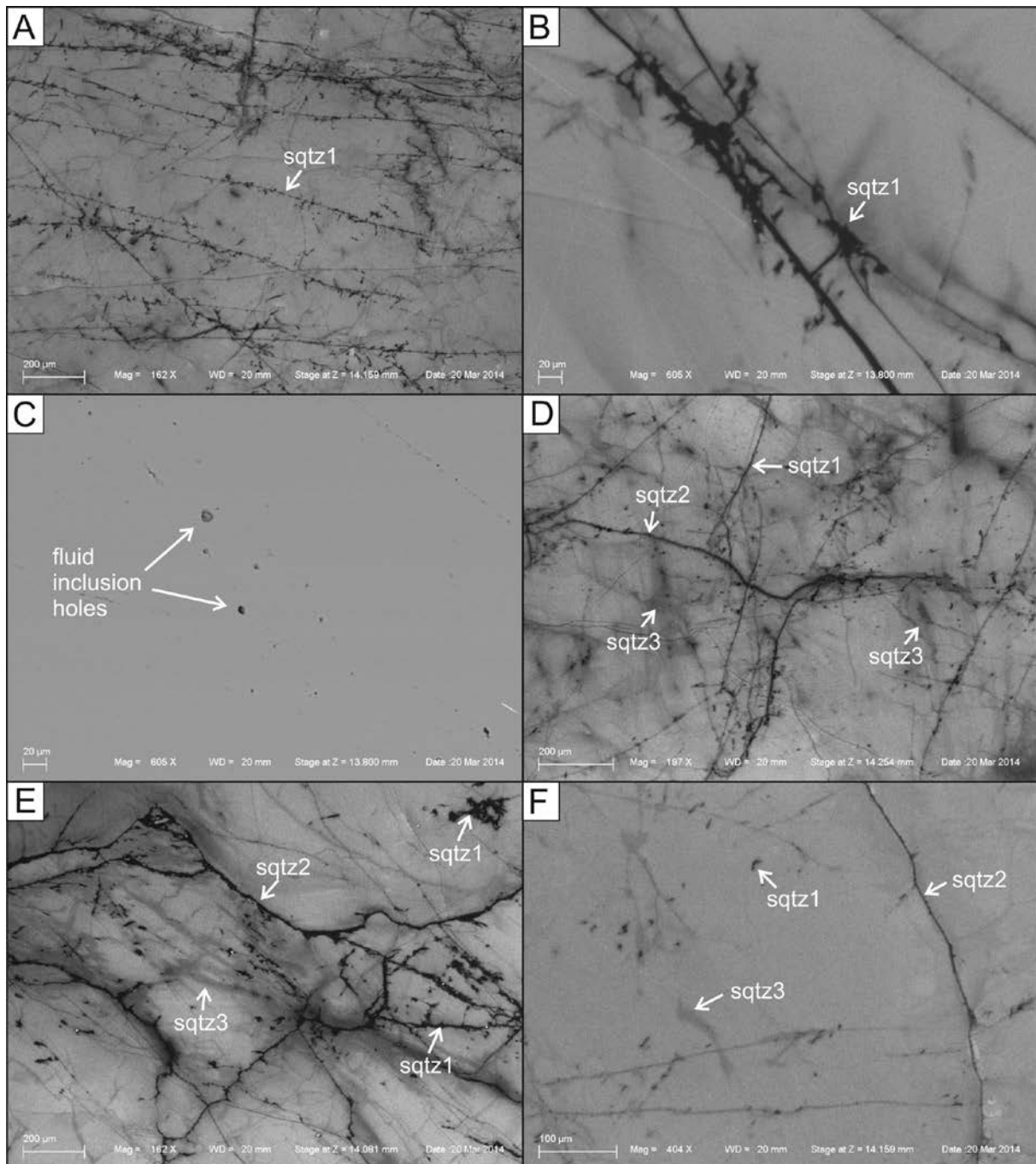


Figure 28. SEM-CL images of quartz. A – Igneous quartz of non-mineralized porphyritic granite from the Synnøve 3 mine, sample 20091308, with bright CL and a network of fractures healed with non-luminescent quartz (sqtz1). B – Close up of a healed fracture (black) containing fluid inclusions. Mineralized pegmatitic quartz band from the Knaben 1 mine. Sample 20091314. C – BSE image of the same crystal as shown in (B) visualizing the holes of decrepitated fluid inclusions which are located within the non-luminescent domains shown in (B). D – Quartz with bright CL with several types of secondary structures (sqtz1 to sqtz3). See text for explanation. Mineralized grey granite from the Knaben 2 mine. Sample 26091311. E – Quartz with bright CL with several types of secondary structures (sqtz1 to sqtz3). See text for explanation. Pegmatite quartz of the Kvina mine. Sample 21091309. D – Quartz with bright CL and a few secondary structures (sqtz1 to sqtz3). See text for explanation. Flaser gneiss of the Knaben 1 mine. Sample 20091313.

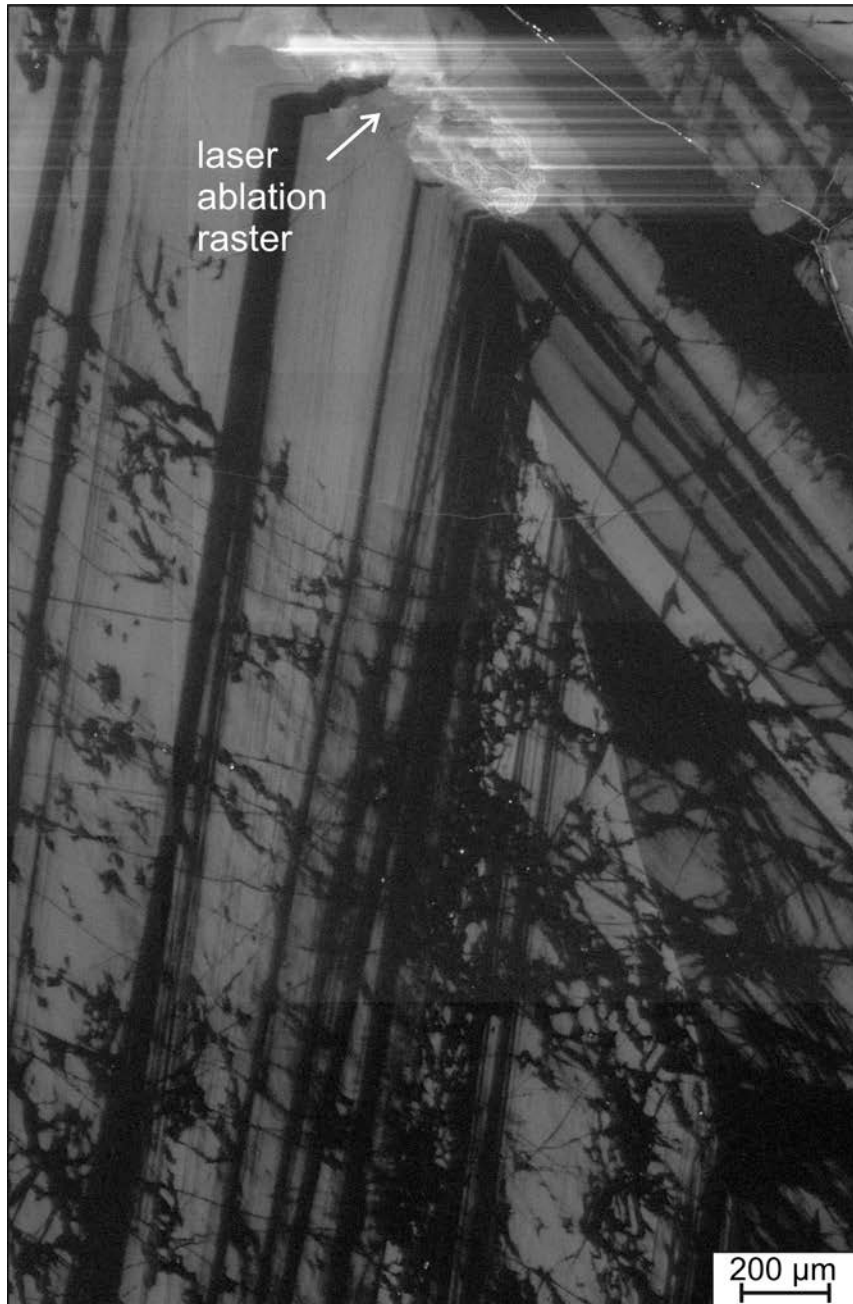


Figure 29. SEM-CL image of a hydrothermal quartz crystals of late, brittle faults exposed in the lower Roma mine (sample 25091307). The crystal shows a distinct primary oscillatory growth zoning (straight banding) overprinted by irregular network of healed, non-luminescent (black) micro fractures connecting micro domains of non-luminescent quartz around fluid inclusions.

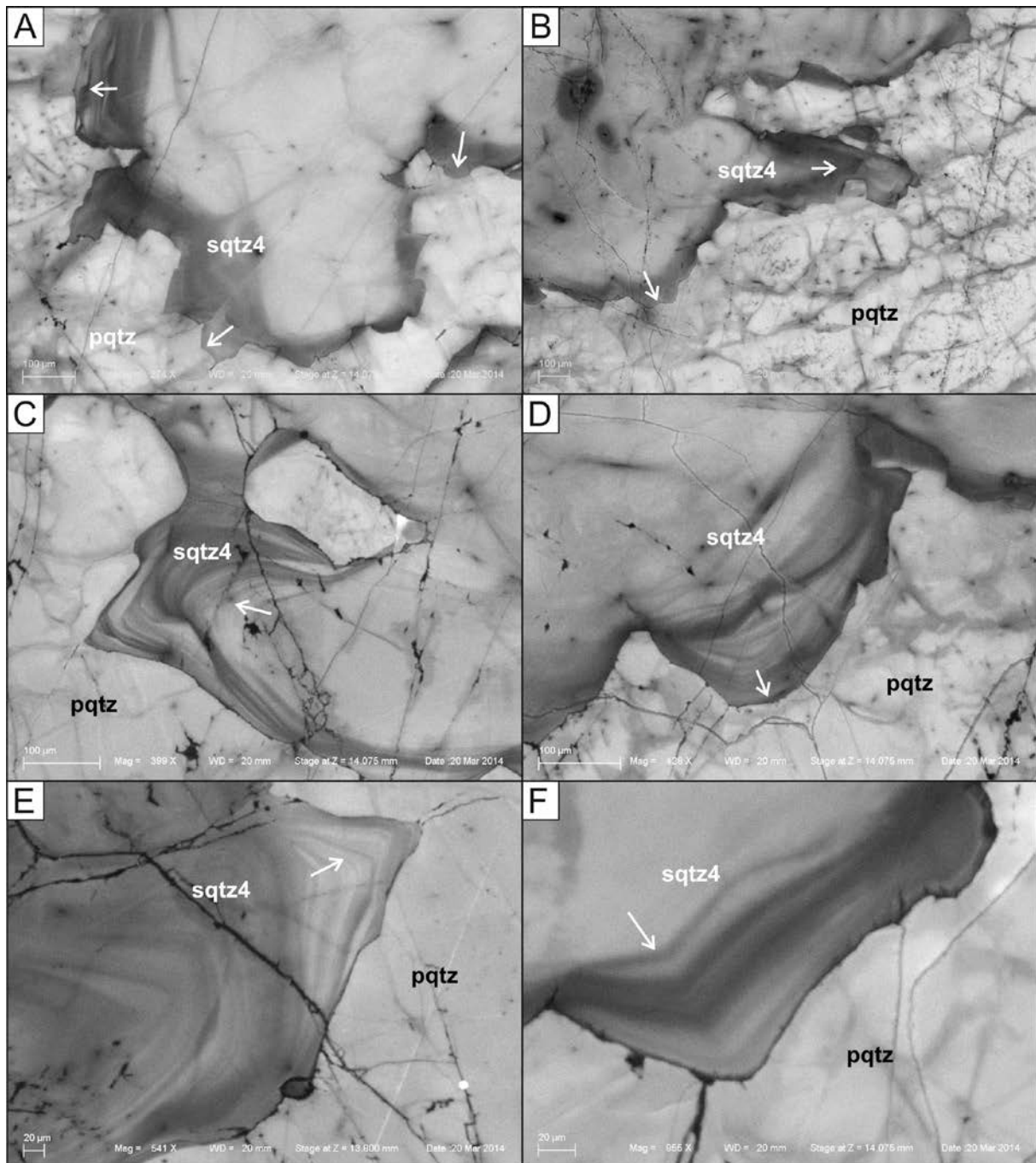


Figure 30. SEM-CL images of secondary quartz *sqtz4* replacing adjacent crystals of primary quartz (*pqtz*) by grain boundary migration. The growth (replacing) direction is indicated by white arrows. A, B, C, D and F - Non-mineralized, undeformed pegmatite from the Knaben 2 mine. Sample 26091308. E - Mineralized pegmatitic quartz band from the Bragold mine. Sample 23091311.

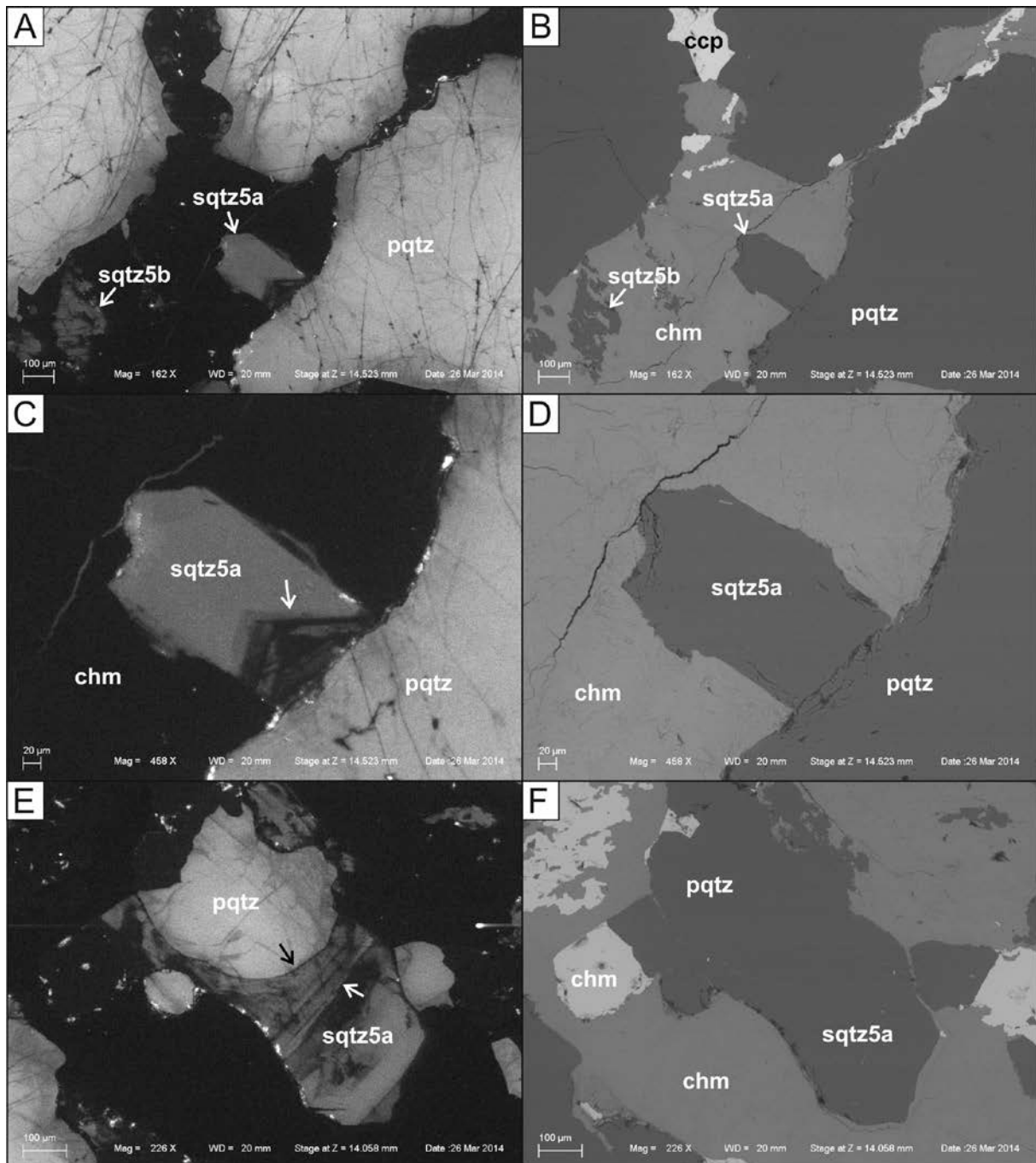


Figure 31. SEM-CL (A, C, D) and BSE (B, D, F) images of quartz of the Hunsbedt Skjærp. The images illustrate how the chalcopyrite (ccp)- chamosite (chm) – apatite (ap) assemblage replaced primary quartz (pqtz) related to the molybdenite mineralization. Minor dull luminescent quartz (sqtz5a and sqtz5b) related to the chalcopyrite mineralization overgrew the primary quartz by forming sub-euhedral crystals (sqtz5a) with growth zoning (white arrows) or dendritic crystals intergrowth with chamosite (sqtz5b). The black arrow in (E) indicates the boundary between primary and secondary quartz overgrowth.

6.2 Quartz chemistry

Concentrations of Li, Be, B, Al, P, Ti, Ca, Na, K, Mn, Fe, and Ge were analyzed *in situ* in individual quartz crystals in different rock types by LA-ICP-MS (Appendix 2). The laser ablation process was observed with a CCD video camera, attached to the laser system, to avoid the ablation and analysis of mineral and fluid micro inclusions commonly occurring in quartz. By doing so, the determined concentrations correspond to the contents of ions which are structurally bound in the quartz lattice.

Al, Ti, Li, and Ge concentrations in quartz of igneous rocks of the Knaben mining district shows a wide scatter typical for differentiated magmatic systems (Müller et al. 2010; Breiter et al. 2013) and references therein) (Figures 32, 33). The data are in range of an earlier trace element study of Knaben quartz by Müller (2006). However, the correlations between these elements which are commonly developed in igneous systems (e.g. Breiter et al. 2013) are only rudimentarily developed in the Knaben samples. The correlations are presumably disturbed due to the long-lived, multiphase magmatism in the area and related multiple, late- to post-magmatic processes. Quartz of the mineralized pegmatitic quartz bands exhibits the widest data scatter and has also the highest average Al (98.2 ± 64.5 ppm) and Li (10.6 ± 4.2 ppm) concentrations (Table 2). Normally the Al and Li content in igneous quartz shows a distinct positive correlation (e.g. Beurlen et al. 2001). In the case of the Knaben samples this trend is only well developed in the quartz with low Al and Li concentrations (non-mineralized, undeformed pegmatites; Figure 33). In the samples with high-Al (>100 ppm) Li is lower compared to “normal” granite and pegmatite quartz (e.g. Beurlen et al. 2011). The reason is simply the generally low Li content of the igneous and mineralized rocks of the Knaben district.

Also the Al versus Ge/Ti graph in Figure 34 shows a disturbed trend, in particular the quartz of the mineralized pegmatitic bands. According to Jacamon and Larsen (2009) the Ge/Ti ratio of quartz is an index of the magmatic evolution of granitic igneous systems and increases exponentially with increasing Al.

Titanium concentrations are relative high, generally >50 ppm except the quartz from the Kvina pegmatite (Table 2), compared to granitic rocks worldwide (e.g. Müller et al. 2010). There seems to be a decrease of the Ti content in the mineralized quartz bands from the south (Bragold mine) towards north (Knaben 1 and Synnøve mines) (Figure 35). However, quartz of the chalcopyrite-molybdenite mineralization at Hunsbedt Skjærp and the pegmatite-hosted Kvina mine do not follow this trend.

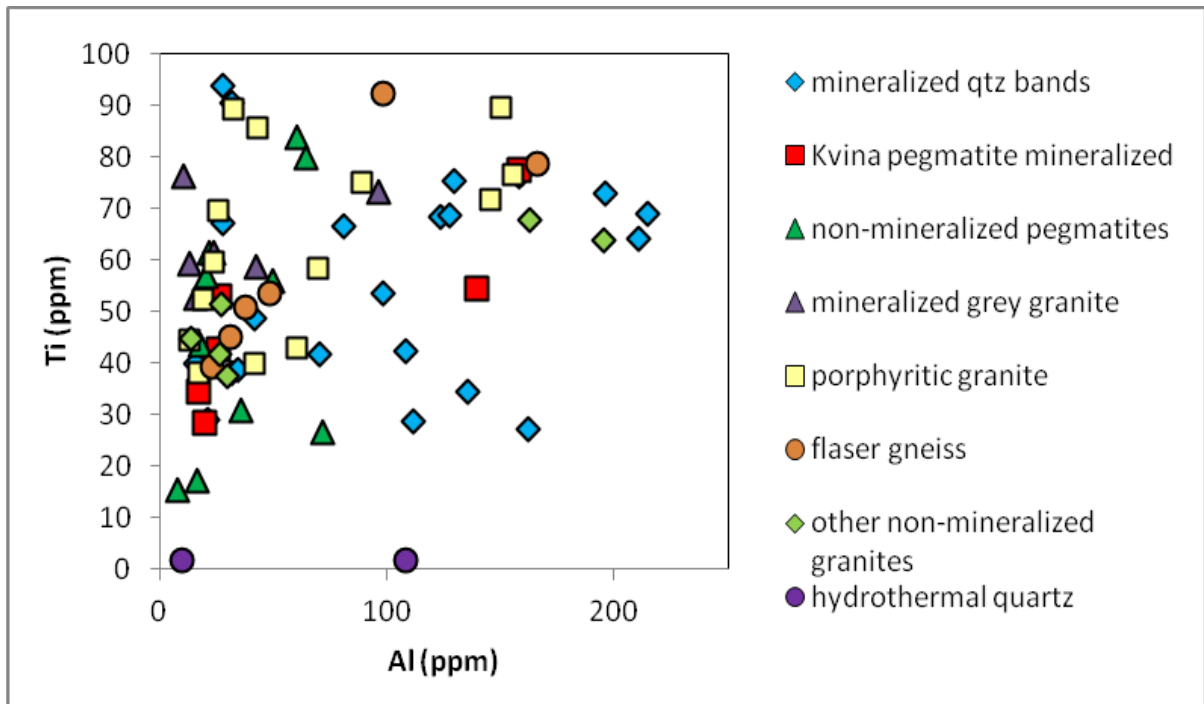


Figure 32. Graph showing Al versus Ti concentrations of investigated quartz samples. Concentrations were determined with LA-ICP-MS.

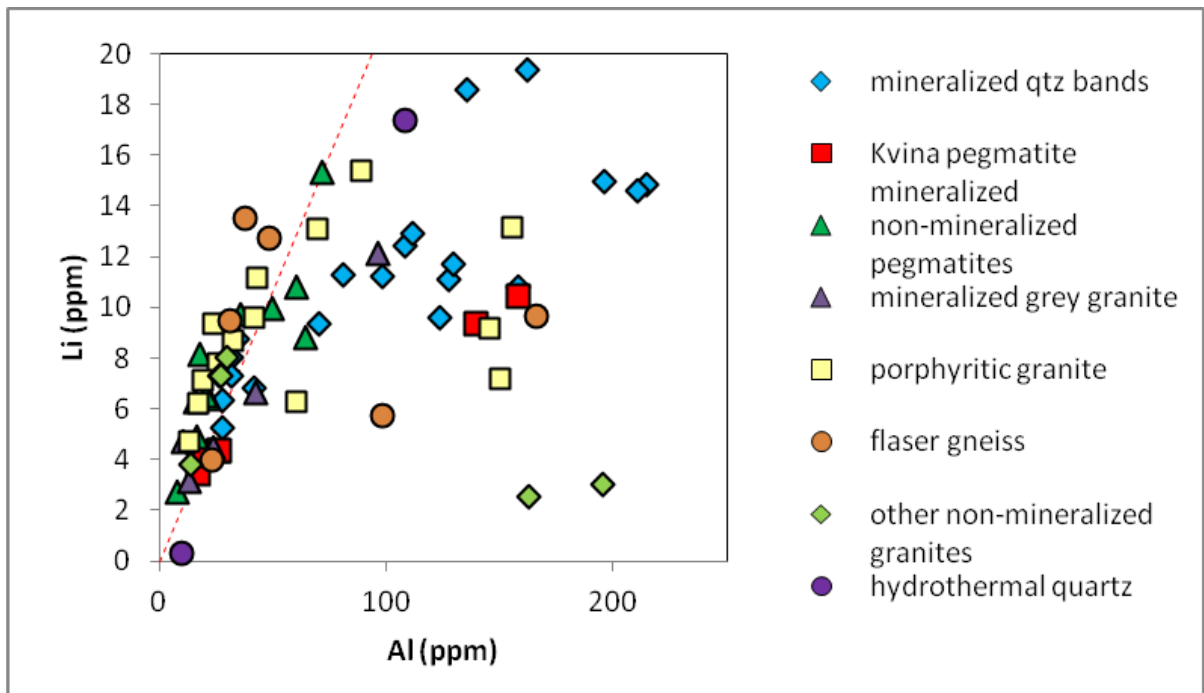


Figure 33. Graph showing Al versus Li concentrations of investigated quartz samples. Concentrations were determined with LA-ICP-MS. The red dashed line corresponds the Al-Li correlation line $Li (ppm) = 0.2133 \times Al (ppm)$ of quartz of the Borborema pegmatites, Brazil, which represents a Li-rich magmatic system (Beurlen et al. 2011).

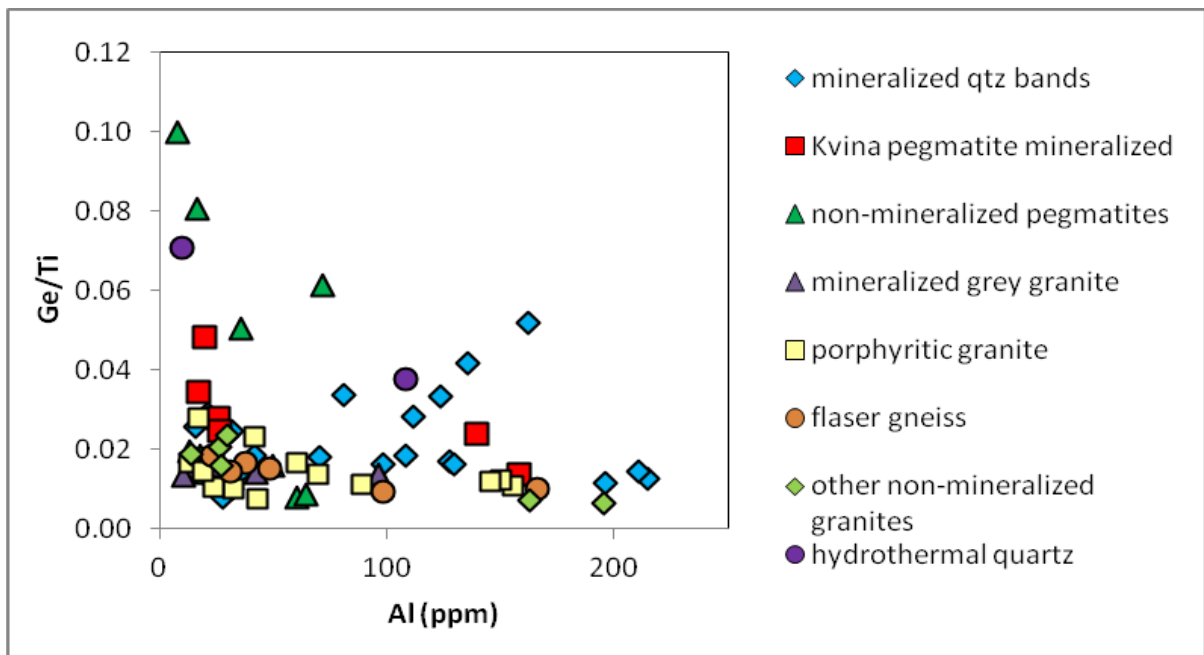


Figure 34. Graph showing the Al concentration versus Ge/Ti ratio of investigated quartz samples. According to Jacamon and Larsen (2009) the Ge/Ti ratio of quartz is an index of the magmatic evolution of granitic igneous systems and, thus, should increase with increasing Al. However, in the case of the Knaben samples no clear trend is developed due to late- to post-magmatic processes. Concentrations were determined with LA-ICP-MS.

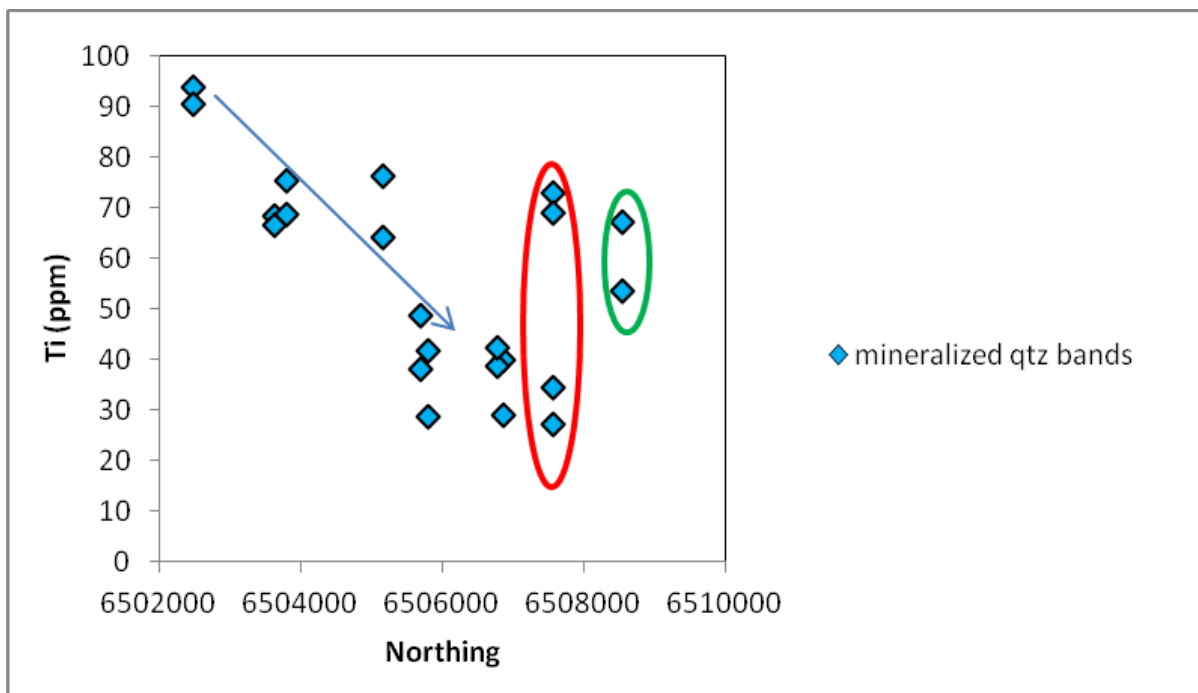


Figure 35. Graph showing the variation of the Ti content of mineralized quartz bands (primary quartz = pqtz) in relation to their N-S location within the Knaben mining district. There seems to be a systematic decrease of the Ti content from the south (Bragold mine) towards north (Knaben 1 and Synnøve mines). Quartz of the chalcopyrite-molybdenite mineralization at Hunsbedt Skjærp (red ellipse) and Kvina mine (green ellipse) do not follow this trend.

Table 2. Average concentrations of trace elements (in ppm) in quartz determined with LA-ICP-MS. Numbers in parentheses correspond to the number of analyses. STD – standard deviation.

		Li	Be	B	Mn	Ge	Rb	Sr	Na	Al	P	K	Ca	Ti	Fe
Mineralized pegmatitic quartz bands	average (22)	10.62	<0.34	<1.64	0.97	1.07	0.57	0.10	34.50	98.17	<7.8	<14.1	<16.9	56.12	11.70
	STD	4.20	-	-	1.27	0.44	1.10	0.06	99.87	64.51	-	-	-	20.19	17.46
Kvina pegmatite	average (6)	9.10	<0.34	<1.64	0.55	1.10	0.14	0.09	5.14	47.61	<7.8	<14.1	<16.9	45.09	11.40
	STD	3.64	-	-	0.57	0.35	0.28	0.04	16.87	33.76	-	-	-	22.76	34.25
Non-mineralized pegmatites	average (12)	6.02	<0.34	<1.64	0.34	1.24	0.52	0.10	15.57	64.24	<7.8	<14.1	<16.9	48.47	1.29
	STD	3.04	-	-	0.13	0.11	0.80	0.08	38.14	65.60	-	-	-	17.48	1.40
Grey, quartz-rich granite	average (6)	6.24	<0.34	<1.64	0.15	0.95	0.01	0.07	8.12	33.40	<7.8	<14.1	<16.9	63.57	2.31
	STD	3.15	-	-	0.12	0.13	0.01	0.02	11.37	32.71	-	-	-	9.19	3.95
Flaser gneiss	average (6)	9.18	<0.34	<1.64	1.08	0.78	0.05	0.09	0.46	67.29	<7.8	<14.1	<16.9	59.94	20.43
	STD	3.75	-	-	1.24	0.08	0.06	0.04	1.13	55.23	-	-	-	20.86	37.37
Reddish porphyritic granite	average (14)	9.21	<0.34	<1.64	0.34	0.83	0.08	0.08	15.52	60.93	<7.8	<14.1	<16.9	65.20	9.08
	STD	3.06	-	-	0.45	0.14	0.10	0.03	45.22	52.69	-	-	-	21.13	15.30
Other non-mineralized granites	average (6)	5.33	<0.34	<1.64	0.22	0.72	0.02	0.08	0.68	75.79	<7.8	<14.1	<16.9	51.10	0.67
	STD	2.57	-	-	0.91	0.18	0.06	0.04	1.31	81.58	-	-	-	15.57	38.28
Hydrothermal quartz	average (2)	8.86	<0.34	<1.64	0.19	0.12	<0.06	0.18	<59.0	58.77	<7.8	<14.1	<16.9	<1.69	<0.61
	STD	12.08	-	-	0.19	0.12	-	0.11	-	69.37	-	-	-	-	-

6.2 Application of the titanium-in-quartz geothermobarometry

The quartz crystallization temperature was calculated applying the Ti-in-quartz geothermobarometer by Huang and Audétat (2012). The applied pressure was 4.0 ± 0.2 kbar based on Al-in-hornblende barometry on porphyritic granite c. 15 km SSW of Knaben (Coint et al. 2015). The applied Ti activity a_{TiO_2} was set at 1, because rutile is a common accessory in the investigated rocks indicating the TiO_2 saturation at least at the time of quartz crystallization. The hydrothermal quartz veins forming brittle, N-S striking fractures are the only samples which do not contain rutile. However, the Ti content of the hydrothermal quartz within the veins is below the detection limit of 1.7 ppm anyway.

The calculated average crystallization temperatures correspond more or less to the crystallization sequence of the Sirdal Magmatic Belt (from high to low temperatures): non-mineralized granites (reddish porphyritic granite), mineralized granites (grey quartz-rich granite), and pegmatites (Table 3). The granitic flaser gneiss, considered as inherited or extrinsic metamagmatic rock not belonging to the Sirdal Magmatic Belt (e.g., Bingen et al. 2015; Coint et al. 2015; Stormoen 2015), has also a high crystallisation temperature of $723\pm 42^\circ\text{C}$. Thus, the rock types related to the molybdenite mineralization were formed at temperatures corresponding to magmatic conditions. The late, non-mineralized hydrothermal quartz veins related to sub-vertical, brittle fracturing have the lowest crystallisation temperature.

The observed decrease of the Ti content of the mineralized quartz bands from south towards north (Figure 35) corresponds to a temperature change from $782\pm 13^\circ\text{C}$ (Bragold mine) to $673\pm 29^\circ\text{C}$ (Knaben 1 and Synnøve mines).

Table 3. Crystallization temperatures of quartz of different rock types of the Knaben mining district. The temperatures were calculated using the Ti-in-quartz geothermobarometer by Huang and Audétat (2012). The applied pressure was 4.0 ± 0.2 kbar based on Al-in-hornblende barometry (Coint et al. 2015). STD – standard deviation.

	nr. of analyses	average	STD
mineralized, ductile deformed pegmatitic quartz bands	22	714	46
mineralized, ductile deformed Kvina pegmatite	6	699	43
non-mineralized, undeformed pegmatites	12	685	61
mineralized grey granite	6	733	21
flaser gneiss	6	723	42
reddish porphyritic granite	14	732	42
other non-mineralized granites	6	707	36
hydrothermal quartz of vertical, N-S striking, brittle faults	2	<440	-

7. Summary and outlook

The results of this study can be summarized as follows:

The major rock type of the Knaben district is weakly foliated, porphyritic reddish biotite granite with an intrusion age of c. 1036 Ma belonging to the Mesoproterozoic Sirdal Magmatic Belt. The porphyritic granite contains commonly ductile deformed mega xenoliths of amphibolite and granitic flaser gneiss in a >10 km long (N-S) and 1 km wide (E-W) belt. This belt corresponds to the area where the molybdenite mineralization occurs. In the Knaben 2 and Ørnehommen mines the porphyritic granite is intruded by grey, quartz-rich granite with fine-grained, disseminated molybdenite. The latter is most likely the primary source of the Mo mineralization (Stormoen 2015 and this study). Coarse-grained molybdenite mineralization is commonly associated with ductile deformed, pegmatitic quartz bands (0.5 to 20 cm wide and up to several meters long) and in one case with a sheet-like, deformed pegmatite (c. 300x150x8 m; Kvina mine). The sequence is cross-cut by undeformed (late), non-mineralized, mostly sub-vertical pegmatite dykes. At the Hunsbedt Skjærp and Kopper Skjærp in the NE of the Knaben mining district the Mo-mineralized pegmatitic quartz bands are partially replaced and superimposed by a chalcopyrite-chamosite-apatite mineralization.

The quartz of almost all investigated mineralized and non-mineralized rock types shows CL features which are typical for igneous quartz. The bright luminescent quartz of the igneous rocks is superimposed by several generations of secondary quartz with low CL intensity. The generally low abundance of secondary structures in the investigated igneous quartz suggests that the amount of circulating, late- to post-magmatic fluids was relative limited. The visualized CL- structures allow in addition the conclusion that no significant quartz deformation (shearing) occurred post-magmatically under retrograde conditions. Thus, the igneous quartz was deformed during the syn-kinematic emplacement of the magmas and the observed foliation in the granites and pegmatites developed from the combination of magmatic and solid state flow.

The most distinctive secondary CL structures are oscillatory growth fronts at quartz crystal margins. The growth fronts form tongues of dull luminescent quartz bulging into and replacing bright luminescent primary quartz by grain boundary migration. Similar structures have been described from amphibolite facies quartzites, i.e. Tverrådalen, Nasafjellet and Melkfjellet in Norway (Müller et al. 2007, 2012). The structures are interpreted as solid-solution replacement structures where crystals with less defects (low CL intensity) replace crystals with higher defect content (high CL intensity). The textures developed presumably post-magmatically during high temperatures which remained over a relative long period allowing the development of these rare textures. Because these textures are omnipresent in all investigated igneous rocks in the Knaben district, they indicate a regional high-temperature event likely caused by long-lasting heat flow and fluid circulation as a result of voluminous, long-lived (c. 1060 to 920 Ma) magmatism related to the Sirdal Magmatic Belt and Hornblende-Biotite Granite Suite (Slagstad et al. 2013; Coint et al. 2015).

Al, Ti, Li, and Ge concentrations in quartz of igneous rocks of the Knaben mining district show a wide scatter. Correlations between these elements are only rudimentarily developed and presumably disturbed by late- to post-magmatic processes as described above. The application of the Ti-in-quartz-geothermobarometer indicates that the rocks associated with the molybdenite mineralization were formed at magmatic conditions at c. 4 kbar. The crystallization temperature of the grey, quartz-rich granite with disseminated molybdenite was $733\pm 21^\circ\text{C}$ and that of the pegmatitic quartz bands with coarse-grained molybdenite mineralization was $714\pm 46^\circ\text{C}$. However, the Ti content of the mineralized quartz bands decreases from south towards north corresponds to a temperature change from $782\pm 13^\circ\text{C}$

(Bragold mine) to $673\pm 29^{\circ}\text{C}$ (Knaben 1 and Synnøve mines). This change may be reflect a continuous temperature gradient of the molybdenite mineralization across the Knaben mining district.

8. References

- Beurlen H., Müller A., Silva D., Da Silva M.R.R. (2011) Petrogenetic significance of trace-element data analyzed with LA-ICP-MS in quartz from the Borborema pegmatite province, northeastern Brazil. *Mineralogical Magazine*, 75: 2703–2719
- Bingen B., Corfu F., Stein H.J., Whitehouse M. (2015) U-Pb geochronology of the syn-orogenic Knaben molybdenum deposits, Sveconorwegian Orogen, Norway. *Geological Magazine* 152: 537-556.
- Breiter K., Ackerman L., Svojtka M., Müller A. (2013) Behavior of trace elements in quartz from plutons of different geochemical signature: A case study from the Bohemian Massif, Czech Republic. *Lithos*, 175–176: 54-67.
- Bugge A. (1963) Norges molybdenforekomster. *Norges Geologiske Undersøkelse* 217: 1-134.
- Coint N., Slagstad T., Roberts N.N.W., Marker M., Røhr T., Sørensen B.E. (2015) The Late Mesoproterozoic Sirdal Magmatic Belt, SW Norway: relationships between magmatism and metamorphism and implications for Sveconorwegian orogenesis. *Precambrian Research*, 265: 57-77.
- Flem B., Müller A. (2012) In situ analysis of trace elements in quartz using laser ablation inductively coupled plasma mass spectrometry. In: Götze J., Möckel R. (eds.) *Quartz: Deposits, mineralogy and analytics*. Springer Geology, Berlin, Heidelberg, p. 219-236.
- Flem B., Larsen R.B., Grimstvedt A., Mansfeld J. (2002) In situ analysis of trace elements in quartz by using laser ablation inductively coupled plasma mass spectrometry. *Chemical Geology* 182: 237–247.
- GeoReM (2011) Geological and environmental reference materials. <<http://georem.mpchmainz.gwdg.de>> Accessed 2 Feb 2014.
- Götze J., Plötze M., Habermann D. (2001) Origin, spectral characteristics and practical applications of the cathodoluminescence (CL) of quartz—a review. *Mineralogy and Petrology* 71: 225–250.
- Huang R., Audétat A. (2012) The titanium-in-quartz (TitaniQ) thermobarometer: A critical examination and re-calibration. *Geochimica et Cosmochimica Acta* 84: 75–89.
- Jacamon F., Larsen R.B. (2009) Trace element evolution of quartz in the charnockitic Kleivan granite, SW-Norway: The Ge/Ti ratio of quartz as an index of igneous differentiation. *Lithos* 107: 281–291.
- Jochum K.P., Weis U., Stoll B., Kuzmin D., Yang Q., Raczek I., Jacob D.E., Stracke A., Birbaum K., Frick D.A., Günther D., Enzweiler J. (2011) Determination of reference values for NIST SRM 610–617 glasses following ISO guidelines. *Geostandards and Geoanalytical Research* 35: 397–429.
- Jourdan C. (2003) Molybdenum mining in the mountains around Knaben. Unpublished report.
- Lysberg K. B. (1976) *Geologi og mineralisering ved Knaben molybdengruber*. Thesis. Universitetet i Bergen. 84 p. (in Norwegian)
- Müller A. (2006) Chemistry of quartz from the Knaben locality. *Norges Geologiske Undersøkelse Rapport* 2006.090.
- Müller A., Ihlen P.M., Wanvik J.E., Flem B. (2007) High-purity quartz mineralisation in kyanite quartzites, Norway. *Mineralium Deposita*, 42: 523-535.
- Müller A., Wiedenbeck M., Flem B., Schiellerup H. (2008) Refinement of phosphorus determination in quartz by LA-ICP-MS through defining new reference material values. *Geostandards and Geoanalytical Research* 32: 361–376.
- Müller A., van den Kerkhof A.M., Behr H.-J., Kronz A., Koch-Müller M. (2010) The evolution of late-Hercynian granites and rhyolites documented by quartz – a review. *Earth and Environmental Science Transactions of the Royal Society of Edinburgh*, vol. 100, pp. 185-204.

- Müller A., Wanvik J. E., Ihlen P.M. (2012) Petrological and chemical characterisation of high-purity quartz deposits with examples from Norway. In: Götze J., Möckel R. (eds.) *Quartz: Deposits, mineralogy and analytics*. Springer Geology, Berlin, Heidelberg, p. 71-118.
- Sandstad J.S. (2012) Agder Mo. In: Eilu P. (ed.) *Mineral deposits and metallogeny of Fennoscandia*. Geological Survey of Finland, Espoo, Special Paper no. 53, pp. 44-54.
- Slagstad T., Roberts N.M.W., Marker M., Røhr T.S., Schiellerup H. (2013) A non-collisional, accretionary Sveconorwegian orogeny. *Terra Nova* 25: 30-37.
- Stormoen M.A. (2015) Synkinematic intrusion of granitoid sheets, with implications for molybdenite deposits in the Knaben Zone, Sirdal Magmatic Belt, SW Norway. M.Sc. thesis, Norwegian University of Science and Technology Trondheim, Norway, 131 p.

Appendix 1. Sample list. Mineral abbreviations: ccp – chalcopyrite, kfs – K-feldspar, mo – molybdenite, py- pyrite, qtz – quartz.

sample nr.	NGU nr.	Rock type	locality	UTM zone	E	N	altitude	method
24091101		mo fracture filling in grey granite	Knaben 2, mining dumps	32V	388310	6503792	662	exhibition
19091301a		grey, quartz-rich mineralized granite with variable grain size and qtz band	Knaben 2, mining dumps	32V	388310	6503792	662	polished slab
19091301b		several mineralized qtz bands in leucocratic granite	Knaben 2, mining dumps	32V	388310	6503792	662	polished slab
19091301c	84678	mineralized qtz band in porphyritic granite	Knaben 2, mining dumps	32V	388310	6503792	662	LA-ICP-MS
20091301		mineralized qtz band (2-5 cm) in porph. granite with mo, py, ccp	Reinshommen hyttefelt, Knaben	32V	388207	6504919	674	
20091302		flaser (tiger stripe) gneiss	Reinshommen, road to Roma mine	32V	388566	6504776	745	
20091203	84679	mineralized qtz band with mo	Roma mine, lower tunnel "Grundstollen"	32V	388886	6505157	764	LA-ICP-MS
20091204		undeformed, discordant, E-W striking pegmatite dyke	track between lower and upper Roma mine	32V	388815	6505578	835	
20091305	84680	mineralized qtz band with mo	Roma mine, upper S tunnel	32V	388831	6505795	839	LA-ICP-MS
20091306a	84681	non-mineralized, undeformed pegmatite vein parallel to mineralized, deformed pegmatitic qtz band	Roma mine, upper S tunnel	32V	388831	6505795	839	LA-ICP-MS
20091306b		mineralized qtz band with marginal, non-mineralized pegmatite, large sample	Roma mine, upper S tunnel	32V	388831	6505795	839	polished slab
20091307		mineralized qtz band with mo	Spillebrot Skjærpene	32V	388913	6506326	850	
20091308	84682	porphyritic granite	Synnøvre 3 mine	32V	388970	6506771	882	LA-ICP-MS
20091309	84683	flaser (tiger stripe) gneiss	Synnøvre 3 mine	32V	388970	6506771	882	LA-ICP-MS
20091310	84684	mineralized qtz band (3-6 cm) with mo	Synnøvre 3 mine	32V	388970	6506771	882	LA-ICP-MS
20091311		concordant massive qtz (1 m), pegmatite?	between Sinnøvre and Knaben 1 mine	32V	388928	6506840	875	
20091312	84685	porphyritic granite	Knaben 1	32V	388760	6506864	874	LA-ICP-MS
20091313	84686	flaser (tiger stripe) gneiss	Knaben 1	32V	388760	6506864	874	LA-ICP-MS
20091314	84687	mineralized qtz band with mo	Knaben 1	32V	388760	6506864	874	LA-ICP-MS
20091315	84688	mineralized qtz with ccp, py, mo	Hunsbedt Skjærp (Mo-Cu mineralization)	32V	389236	6507570	876	LA-ICP-MS
20091316	84689	"specky" qtz	Hunsbedt Skjærp (Mo-Cu mineralization)	32V	389236	6507570	876	LA-ICP-MS
20091317		brecciated, mineralized qtz with ccp, py, large sample	Hunsbedt Skjærp (Mo-Cu mineralization)	32V	389236	6507570	876	polished slab
21091301		mineralized qtz band with mo	Kvina mine	32V	389103	6508551	871	
21091302	84690	mineralized qtz band with mo	Kvina mine	32V	389103	6508551	871	LA-ICP-MS
21091303	84691	discordant, non-mineralized pegmatite dyke	Kvina mine	32V	389103	6508551	871	LA-ICP-MS

Appendix 1. Continued.

sample nr.	NGU nr.	Rock type	locality	UTM zone	E	N	altitude	method
21091304	84692	porphyritic granite	Kvina mine	32V	389103	6508551	871	LA-ICP-MS
21091305		qtz of large deformed pegmatite	Kvina mine	32V	389103	6508551	871	
21091306a		mineralized deformed pegmatite (Kfs), large sample	Kvina mine	32V	389103	6508551	871	exhibition
21091306b		mineralized deformed pegmatite (kfs, qtz, bt), large sample	Kvina mine	32V	389103	6508551	871	exhibition
21091307	84693	qtz of large deformed pegmatite	Kvina mine	32V	389103	6508551	871	LA-ICP-MS
21091308	84694	qtz of large deformed pegmatite	Kvina mine	32V	389103	6508551	871	LA-ICP-MS
21091309	84695	qtz of large deformed pegmatite	Kvina mine	32V	389103	6508551	871	LA-ICP-MS
23091301	84696	porphyritic granite	Ørnehommen mine, upper tunnel	32V	387924	6505700	719	LA-ICP-MS
23091302	84697	qtz band with no visible mineralization	Ørnehommen mine, upper tunnel	32V	387924	6505700	719	LA-ICP-MS
23091303	84698	non-mineralized, fine-grained grey granite	Ørnehommen mine, upper tunnel	32V	387924	6505700	719	LA-ICP-MS
23091304		discordant, non-mineralized pegmatite dyke	Upper Reinshommen mine	32V	388726	6505463	806	
23091306		mineralized qtz band (2-8 cm) with mo	Hommen mine	32V	388130	6502372	731	
23091307		qtz band with no visible mineralization	Bragold mine	32V	387250	6502486	694	
23091308		mineralized qtz band (2-20 cm) with mo	Bragold mine	32V	387250	6502486	694	
23091309		mineralized qtz band (2-20 cm) with mo	Bragold mine	32V	387250	6502486	694	
23091310		mineralized qtz band (2-20 cm) with mo	Bragold mine	32V	387250	6502486	694	
23091311	84699	mineralized qtz band (2-20 cm) with mo, large sample	Bragold mine	32V	387250	6502486	694	LA-ICP-MS
23091312		qtz band with no visible mineralization	Bragold mine	32V	387250	6502486	694	
23091313	84700	porphyritic granite	Bragold mine	32V	387250	6502486	694	LA-ICP-MS
24091301		discordant, non-mineralized pegmatite dyke	300 m ESE of Kvina mine	32V	389428	6508369	849	
24091302		concordant, non-mineralized qtz band (2-6 cm)	300 m ESE of Kvina mine	32V	389428	6508369	849	
24091303	84701	non-mineralized pegmatite qtz, large concordant Kfs-pegmatite	1 km ESE of Kvina mine	32V	390193	6508186	933	LA-ICP-MS
24091304	84702	porphyritic granite, far away of mineralization	1 km ESE of Kvina mine	32V	390145	6508035	915	LA-ICP-MS
24091305		mineralized qtz band with mol	Spillebrot Skjærpene mine, E tunnel	32V	389016	6506801	875	
24091306		porphyritic granite	Spillebrot Skjærpene mine, E tunnel	32V	389016	6506801	875	
24091307		flaser (tiger stripe) gneiss	Spillebrot Skjærpene mine, E tunnel	32V	389016	6506801	875	

Appendix 1. Continued.

sample nr.	NGU nr.	Rock type	locality	UTM zone	E	N	altitude	method
24091308	84703	discordant, non-mineralized pegmatite dyke	Knaben 1	32V	388760	6506864	874	LA-ICP-MS
24091309		mineralized qtz band with mol	Knaben 1	32V	388760	6506864	874	
24091310		mineralized aplite (continuation of qtz band) with mo	Knaben 1	32V	388760	6506864	874	exhibition
24091311		massive mol from qtz band 250 g	Knaben 1	32V	388760	6506864	874	
25091301		contact medium-grained porphyritic granite/fine-grained grey granite (non-mineralized)	Ørnehommen mine, lower tunnel	32V	387895	6505669	700	polished slab
25091302	84704	non-mineralized, discordant white medium-grained granite (alaskite)	Ørnehommen mine, lower tunnel	32V	387895	6505669	700	LA-ICP-MS
25091303		non-mineralized, concordant fine-grained grey granite	Ørnehommen mine, lower tunnel	32V	387895	6505669	700	
25091304	84705	concordant, mineralized, medium-grained leucocratic granite	Ørnehommen mine, upper tunnel	32V	387924	6505700	719	LA-ICP-MS, Trond Slagstad
25091305	84706	discordant, non-mineralized pegmatite dyke	Ørnehommen mine, upper tunnel	32V	387924	6505700	719	LA-ICP-MS
25091306		contact porphyritic granite/medium-grained leucocratic granite (mineralized)	Ørnehommen mine, upper tunnel	32V	387924	6505700	719	polished slab
25091307	84707	late, vertical shear zone with hydrothermal qtz	Roma mine, lower tunnel "Grundstollen"	32V	388886	6505157	764	LA-ICP-MS
25091308	84708	porphyritic granite	Roma mine, lower tunnel "Grundstollen"	32V	388886	6505157	764	LA-ICP-MS
25091309	84709	flaser (tiger stripe) gneiss	Roma mine, lower tunnel "Grundstollen"	32V	388886	6505157	764	LA-ICP-MS
26091301		mineralized qtz band with mo	Jelå mine	32V	388050	6505574	772	
26091302		porphyritic granite	Jelå mine	32V	388050	6505574	772	
26091303		vertical E-W dolerite dyke (15 m wide)	Jelå mine	32V	388050	6505574	772	Trond Slagstad
26091304		contact/transition porphyritic granite/flaser (tiger stripe) gneiss	Roma mine, upper S tunnel	32V	388831	6505795	839	polished slab
26091305	84710	dark bt granite, large body (enclave?) in porphyritic granite	Roma mine, upper N tunnel	32V	388845	6505823	840	LA-ICP-MS, Trond Slagstad
26091306		contact porphyritic granite/dark biotite granite	Roma mine, upper N tunnel	32V	388845	6505823	840	polished slab
26091307		mineralized qtz band with mo	Knaben 2	32V	388271	6503630	679	
26091308	84711	concordant pegmatite veins in medium-grained leucocratic granite (mineralized)	Knaben 2	32V	388271	6503630	679	LA-ICP-MS
26091309		concordant pegmatite veins in medium-grained leucocratic granite (mineralized)	Knaben 2	32V	388271	6503630	679	
26091310	84712	medium-grained leucocratic granite (mineralized)	Knaben 2	32V	388271	6503630	679	LA-ICP-MS

Appendix 1. Continued.

sample nr.	NGU nr.	Rock type	locality	UTM zone	E	N	altitude	method
26091311	84713	medium-grained leucocratic granite (mineralized)	Knaben 2	32V	388271	6503630	679	LA-ICP-MS
26091312	84714	undeformed, concordant pegmatite vein in porphyritic granite	Knaben 2	32V	388271	6503630	679	LA-ICP-MS
26091313		mineralized qtz band (pegmatite) with lot of mo	Knaben 2	32V	388271	6503630	679	exhibition

Appendix 2. Trace element concentrations (in ppm) of quartz determined with LA-ICP-MS. Two analyses (A and B) were performed on each sample. Concentrations of Na, K, and Ca above the limit of detection (LOD) are caused by fluid inclusions. Rock type abbreviations: fgn – flaser gneiss, ggr – mineralized grey granite, hqtz – hydrothermal quartz of late fractures, mo-qtz – mineralized pegmatitic quartz bands, ngr - non-mineralized granites except prophyritic granite, pegd - non-mineralized pegmatite dykes, peg – Kvina pegmatite, pgr – porphyritic granite.

locality	Rock type	LOD	Li	Be	B	Mn	Ge	Rb	Sr	Na	Al	P	K	Ca	Ti	Fe
			0.33	0.34	1.64	0.06	0.07	0.06	0.01	59.0	6.3	7.8	14.1	16.9	1.69	0.61
Knaben 2	mo-qtz	19091301-A	11.72	<0.34	<1.64	1.19	1.22	4.84	0.12	<59.0	129.2	<7.8	85.2	26.4	75.30	8.75
		19091301-B	11.09	<0.34	<1.64	0.63	1.17	1.77	0.17	<59.0	127.4	<7.8	<14.1	<16.9	68.50	3.21
Roma, lower tunnel	mo-qtz	20091303-A	14.61	<0.34	<1.64	2.62	0.93	0.17	0.06	<59.0	210.9	<7.8	25.0	<16.9	64.08	20.33
		20091303-B	10.78	<0.34	<1.64	1.61	0.95	1.07	0.09	<59.0	158.0	<7.8	44.9	<16.9	76.07	24.95
Roma, upper S tunnel	mo-qtz	20091305-A	9.35	<0.34	<1.64	0.85	0.75	<0.06	0.04	<59.0	70.2	<7.8	<14.1	<16.9	41.78	47.35
		20091305-B	12.92	<0.34	<1.64	5.69	0.81	<0.06	0.06	<59.0	111.4	<7.8	<14.1	57.5	28.69	70.67
Roma, upper S tunnel	pegd	20091306-A	13.33	<0.34	<1.64	0.70	0.96	<0.06	0.09	<59.0	93.9	<7.8	<14.1	<16.9	31.64	6.02
		20091306-B	12.59	<0.34	<1.64	2.00	1.27	<0.06	0.11	<59.0	113.4	<7.8	<14.1	46.9	38.19	119.90
Synnøvre 3	pgr	20091308-A	13.12	<0.34	<1.64	<0.06	0.80	0.20	0.09	171.2	69.4	<7.8	23.2	<16.9	58.34	3.33
		20091308-B	11.15	<0.34	<1.64	0.19	0.64	<0.06	0.13	<59.0	42.8	<7.8	<14.1	<16.9	85.54	1.55
Synnøvre 3	fgn	20091309-A	3.97	<0.34	<1.64	0.17	0.72	<0.06	0.05	<59.0	22.8	<7.8	<14.1	<16.9	39.15	<0.61
		20091309-B	9.48	<0.34	<1.64	0.27	0.65	<0.06	0.07	<59.0	30.9	<7.8	<14.1	<16.9	45.08	1.15
Synnøvre 3	mo-qtz	20091310-A	12.42	<0.34	<1.64	<0.06	0.78	0.41	0.11	456.5	108.3	<7.8	42.9	<16.9	42.26	4.68
		20091310-B	8.75	<0.34	<1.64	<0.06	0.53	0.22	0.30	76.9	34.1	8.7	<14.1	<16.9	38.82	0.74
Knaben 1	pgr	20091312-A	7.12	<0.34	<1.64	0.17	0.76	<0.06	0.08	<59.0	19.1	<7.8	<14.1	<16.9	52.43	<0.61
		20091312-B	4.68	<0.34	<1.64	0.30	0.73	<0.06	0.09	<59.0	12.8	<7.8	<14.1	<16.9	44.53	<0.61
Knaben 1	fgn	20091313-A	12.72	<0.34	<1.64	0.34	0.82	0.10	0.07	<59.0	48.4	<7.8	<14.1	<16.9	53.63	1.41
		20091313-B	13.51	<0.34	<1.64	0.37	0.84	<0.06	0.09	<59.0	37.4	<7.8	<14.1	<16.9	50.82	0.72
Knaben 1	mo-qtz	20091314-A	4.32	<0.34	<1.64	0.27	1.02	<0.06	0.07	<59.0	15.4	<7.8	<14.1	<16.9	39.81	<0.61
		20091314-B	4.10	<0.34	<1.64	0.33	0.84	<0.06	0.07	<59.0	20.9	<7.8	<14.1	<16.9	29.02	<0.61
Hunsbedt Skjærp	mo-qtz	20091315-A	14.82	<0.34	<1.64	0.70	0.88	0.21	0.10	96.9	214.9	<7.8	21.9	<16.9	68.88	13.77
		20091315-B	14.96	<0.34	<1.64	2.38	0.86	0.16	0.09	<59.0	196.1	<7.8	15.9	<16.9	72.92	9.22
Hunsbedt Skjærp	mo-qtz	20091316-A	18.57	<0.34	<1.64	<0.06	1.44	<0.06	0.08	108.7	135.2	<7.8	14.7	<16.9	34.49	21.43
		20091316-B	19.39	<0.34	1.68	1.42	1.41	0.18	0.08	<59.0	161.8	<7.8	16.7	<16.9	27.10	14.11

Appendix 2. Continued.

locality	Rock type	LOD	Li	Be	B	Mn	Ge	Rb	Sr	Na	Al	P	K	Ca	Ti	Fe
			0.33	0.34	1.64	0.06	0.07	0.06	0.01	59.0	6.3	7.8	14.1	16.9	1.69	0.61
Kvina	mo-qtz	21091302-A	11.21	<0.34	<1.64	0.69	0.87	0.28	0.14	<59.0	98.2	<7.8	16.4	<16.9	53.64	1.85
		21091302-B	5.28	<0.34	<1.64	0.21	0.93	<0.06	0.08	<59.0	27.5	<7.8	<14.1	<16.9	67.22	<0.61
Kvina e	pegd	21091303-A	8.84	<0.34	<1.64	0.27	0.71	0.08	0.12	<59.0	64.0	<7.8	<14.1	<16.9	79.99	<0.61
		21091303-B	10.78	<0.34	<1.64	0.75	0.65	0.66	0.18	<59.0	60.2	<7.8	19.5	17.0	83.90	2.24
Kvina	pgr	21091304-A	6.28	<0.34	<1.64	0.25	0.72	<0.06	0.14	<59.0	23.8	<7.8	<14.1	21.4	42.88	<0.61
		21091304-B	9.35	<0.34	<1.64	0.34	0.62	<0.06	0.06	<59.0	28.9	<7.8	<14.1	<16.9	59.57	<0.61
Kvina	peg	21091307-A	4.37	<0.34	<1.64	0.30	1.30	<0.06	0.07	<59.0	26.1	<7.8	<14.1	<16.9	53.06	0.90
		21091307-B	4.35	<0.34	<1.64	0.31	1.19	<0.06	0.05	<59.0	25.6	<7.8	<14.1	<16.9	42.69	<0.61
Kvina	peg	21091308-A	9.34	<0.34	<1.64	0.52	1.31	1.76	0.21	<59.0	139.2	<7.8	62.8	29.4	54.49	2.79
		21091308-B	10.45	<0.34	<1.64	0.47	1.07	1.34	0.19	<59.0	157.7	<7.8	92.6	18.7	77.52	3.32
Kvina	peg	21091309-A	4.16	<0.34	<1.64	0.16	1.37	<0.06	0.02	<59.0	19.7	<7.8	<14.1	<16.9	28.43	<0.61
		21091309-B	3.46	<0.34	<1.64	0.27	1.19	<0.06	0.05	<59.0	17.1	<7.8	<14.1	22.4	34.60	<0.61
Ørnehommen, upper tunnel	pgr	23091301-A	6.22	<0.34	<1.64	0.28	1.06	<0.06	0.05	<59.0	17.1	<7.8	<14.1	<16.9	37.96	<0.61
		23091301-B	9.62	<0.34	<1.64	<0.06	0.93	<0.06	0.05	<59.0	41.5	8.8	<14.1	<16.9	39.95	<0.61
Ørnehommen, upper tunnel	mo-qtz	23091302-A	6.83	<0.34	<1.64	0.19	0.90	<0.06	0.04	<59.0	31.3	<7.8	<14.1	<16.9	48.63	<0.61
		23091302-B	7.28	<0.34	<1.64	0.28	0.94	<0.06	0.06	<59.0	45.8	<7.8	<14.1	<16.9	38.06	1.01
Ørnehommen, upper tunnel	ngr	23091303-A	8.04	<0.34	<1.64	0.30	0.88	<0.06	0.07	<59.0	29.7	<7.8	<14.1	<16.9	37.44	<0.61
		23091303-B	7.29	<0.34	<1.64	0.28	0.81	<0.06	0.05	<59.0	26.9	<7.8	<14.1	<16.9	51.27	<0.61
Bragold	mo-qtz	23091311-A	8.04	<0.34	3.10	0.80	0.93	1.01	0.17	<59.0	31.2	<7.8	<14.1	<16.9	90.52	0.65
		23091311-B	6.36	<0.34	<1.64	0.39	0.75	<0.06	0.07	<59.0	27.3	<7.8	<14.1	<16.9	93.73	<0.61
Bragold	pgr	23091313-A	8.67	<0.34	<1.64	<0.06	0.92	<0.06	0.10	<59.0	32.3	<7.8	<14.1	<16.9	89.37	<0.61
		23091313-B	7.80	<0.34	<1.64	<0.06	0.76	<0.06	0.09	<59.0	25.4	<7.8	<14.1	<16.9	69.41	<0.61
1 km ESE of Kvina	pegd	24091303-A	2.71	<0.34	<1.64	0.27	1.53	<0.06	0.06	<59.0	7.5	<7.8	<14.1	<16.9	15.28	<0.61
		24091303-B	4.90	<0.34	<1.64	0.40	1.38	<0.06	0.05	<59.0	16.4	<7.8	<14.1	<16.9	17.08	<0.61
1 km ESE of Kvina	pgr	24091304-A	9.18	<0.34	<1.64	0.82	0.86	0.16	0.08	<59.0	145.5	<7.8	37.2	<16.9	71.61	34.72
		24091304-B	7.19	<0.34	<1.64	1.48	1.10	0.34	0.07	<59.0	150.3	<7.8	25.5	<16.9	89.66	36.01

Appendix 2. Continued.

locality	Rock type	LOD	Li	Be	B	Mn	Ge	Rb	Sr	Na	Al	P	K	Ca	Ti	Fe
			0.33	0.34	1.64	0.06	0.07	0.06	0.01	59.0	6.3	7.8	14.1	16.9	1.69	0.61
Knaben 1	pegd	24091308-A	8.13	<0.34	<1.64	0.24	0.81	<0.06	0.04	<59.0	17.4	<7.8	<14.1	<16.9	43.52	<0.61
		24091308-B	6.52	<0.34	<1.64	0.37	0.80	<0.06	0.09	<59.0	20.1	<7.8	<14.1	<16.9	56.88	<0.61
Ørnehommen, lower tunnel	ngr	25091302-A	3.79	<0.34	<1.64	0.18	0.85	<0.06	0.06	<59.0	13.7	<7.8	<14.1	<16.9	44.88	<0.61
		25091302-B	7.29	<0.34	<1.64	0.24	0.86	<0.06	0.09	<59.0	26.4	<7.8	<14.1	<16.9	41.71	<0.61
Ørnehommen, upper tunnel	ggr	25091304-A	4.74	<0.34	<1.64	0.21	1.01	<0.06	0.08	<59.0	10.2	<7.8	<14.1	<16.9	76.29	<0.61
		25091304-B	6.30	<0.34	<1.64	0.23	0.82	<0.06	0.07	<59.0	15.7	<7.8	<14.1	<16.9	52.50	<0.61
Ørnehommen, upper tunnel	pegd	25091305-A	6.42	<0.34	<1.64	<0.06	1.01	<0.06	0.06	<59.0	21.5	<7.8	<14.1	<16.9	61.43	<0.61
		25091305-B	9.98	<0.34	<1.64	0.11	0.89	<0.06	0.08	<59.0	49.5	<7.8	<14.1	<16.9	55.92	0.69
Roma, lower tunnel	hqtz	25091307-A	17.40	<0.34	<1.64	0.19	<0.07	<0.06	0.10	<59.0	107.8	<7.8	<14.1	<16.9	<1.69	<0.61
		25091307-B	0.31	<0.34	<1.64	<0.06	0.12	0.09	0.26	121.0	9.7	<7.8	<14.1	34.4	<1.69	<0.61
Roma, lower tunnel	pgr	25091308-A	15.38	<0.34	<1.64	1.00	0.83	<0.06	0.06	<59.0	88.7	<7.8	<14.1	<16.9	75.03	10.80
		25091308-B	13.18	<0.34	<1.64	<0.06	0.84	0.13	0.05	<59.0	155.4	9.4	23.0	<16.9	76.56	39.55
Roma, lower tunnel	fgn	25091309-A	5.75	<0.34	<1.64	2.91	0.85	<0.06	0.11	<59.0	98.3	<7.8	<14.1	<16.9	92.30	24.96
		25091309-B	9.66	<0.34	<1.64	2.43	0.79	0.15	0.15	<59.0	165.9	<7.8	25.9	21.8	78.69	94.13
Roma, upper N tunnel	ngr	26091305-A	3.03	<0.34	<1.64	0.09	0.42	<0.06	0.10	<59.0	195.6	<7.8	17.8	20.7	63.70	1.42
		26091305-B	2.56	<0.34	<1.64	0.21	0.48	0.13	0.09	<59.0	162.5	<7.8	15.7	<16.9	67.61	2.14
Knaben 2	mo-qtz	26091308-A	11.31	<0.34	<1.64	0.51	2.25	0.23	0.09	<59.0	81.1	<7.8	18.2	<16.9	66.63	3.96
		26091308-B	9.59	<0.34	<1.64	0.51	2.27	1.92	0.10	<59.0	123.4	<7.8	42.1	<16.9	68.44	8.96
Knaben 2	ggr	26091310-A	4.46	<0.34	<1.64	<0.06	0.87	<0.06	0.09	<59.0	23.6	<7.8	<14.1	<16.9	61.46	<0.61
		26091310-B	3.17	<0.34	<1.64	0.20	1.16	<0.06	0.05	<59.0	13.0	<7.8	<14.1	<16.9	59.30	<0.61
Knaben 2	ggr	26091311-A	12.11	<0.34	<1.64	0.27	1.01	<0.06	0.08	<59.0	96.0	<7.8	<14.1	<16.9	73.14	3.46
		26091311-B	6.67	<0.34	<1.64	0.06	0.84	<0.06	0.05	<59.0	42.0	<7.8	<14.1	<16.9	58.71	9.91
Knaben 2	pegd	26091312-A	9.71	<0.34	<1.64	0.26	1.55	<0.06	0.05	<59.0	35.8	<7.8	<14.1	<16.9	30.72	<0.61
		26091312-B	15.30	<0.34	<1.64	1.24	1.63	0.81	0.13	<59.0	71.5	<7.8	<14.1	<16.9	26.59	6.98



GEOLOGICAL
SURVEY OF
NORWAY

· NGU ·

Geological Survey of Norway
PO Box 6315, Sluppen
N-7491 Trondheim, Norway

Visitor address
Leiv Eirikssons vei 39
7040 Trondheim

Tel (+ 47) 73 90 40 00
E-mail ngu@ngu.no
Web www.ngu.no/en-gb/